

Spiro[1,2]oxaphosphetanes of Non-stabilized and Semi-stabilized Phosphorus Ylide Derivatives. Synthesis and Kinetic and Computational Study of their Thermolysis

Jesús García López,^a Pablo M. Sansores Peraza,^a María José Iglesias,^a Laura

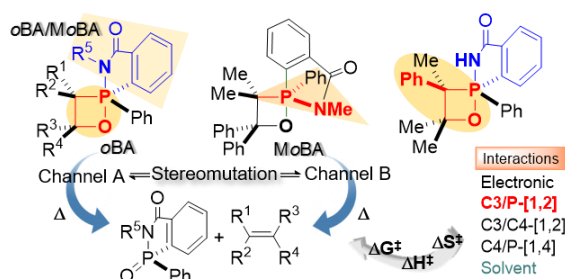
Roces,^{b,c} Santiago García-Granda,^b Fernando López Ortiz^{*a}

^a Área de Química Orgánica, Centro de Investigación CIAIMBITAL, Universidad de Almería, 04120 Almería, Spain. Tel: +34950015478. flortiz@ual.es

^b Departamento de Química Física y Analítica, Universidad de Oviedo-CINN, C/ Julián Clavería 8, 33006 Oviedo, Spain.

^c Servicios Científico Técnicos, Universidad de Oviedo, 33006 Oviedo, Spain.

Abstract Graphic



Abstract. A series of tri- and tetra-substituted spiro-oxaphosphetanes stabilized by *ortho*-benzamide (*oBA*) and *N*-methyl *ortho*-benzamide (*MoBA*) ligands have been synthesized by reaction of C_{α},C_{ortho} dilithiated phosphazenes with aldehydes and ketones. They include enantiopure products and the first example of an isolated oxaphosphetane having a phenyl substituent at C3 of the ring. Kinetic studies of their thermal decomposition evidenced that the process takes place irreversibly through a polar transition state ($\rho = -0.22$) under the influence of electronic, [1,2], [1,3] steric and solvent effects, being C3/P-[1,2] interactions the largest contribution to ΔG^{\ddagger} of olefination. Inversion of the phosphorus configuration through stereomutation has been observed in a number of cases. DFT calculations showed that *oBA* derivatives olefinated through the isolated (N, O)(Ph, C₆H₄, C) oxaphosphetanes (Channel A), whereas *MoBA* compounds decomposed faster via the isomer (C₆H₄, O)(C, N, Ph) formed by P-stereomutation involving a M_{B2} permutational mechanism (Channel B). The energy barrier of P-isomerization is lower than that of olefination. Fragmentation takes place in a concerted asynchronous reaction. The thermal stability of oxaphosphetanes is determined by strong

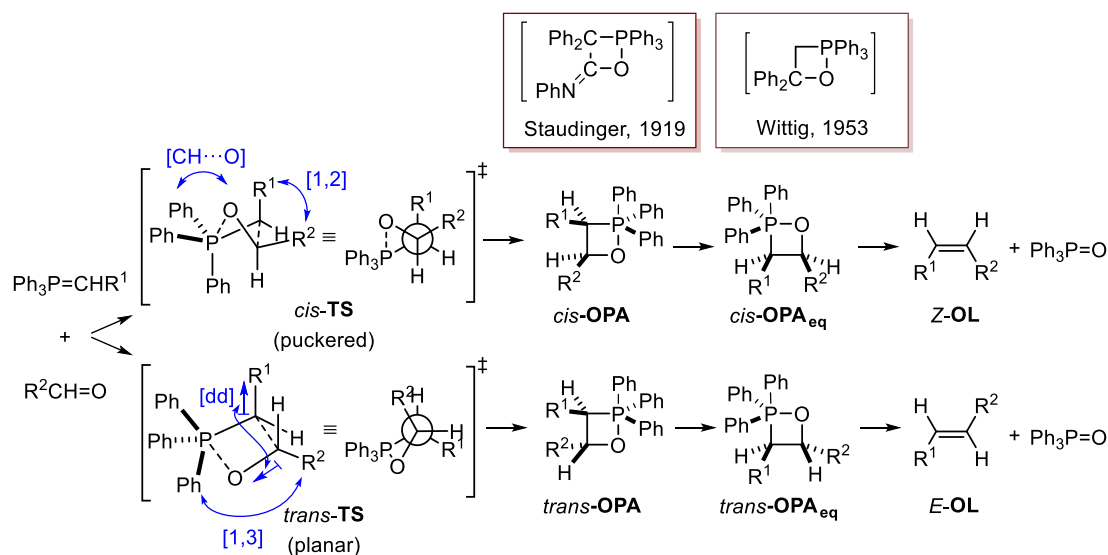
C3/P-[1,2] interactions destabilizing the transition state of olefination. The effect of charge distribution, C3/C4-[1,2], and C4/P-[1,3] steric and solvent interactions on ΔG^\ddagger were also evaluated.

Introduction

In 1919, Staudinger and Meyer found that the reaction of $\text{Ph}_3\text{P}=\text{CPh}_2$ with phenylisocyanate afforded triphenylketenimine and triphenylphosphine oxide and suggested the involvement of a 1,2-oxaphosphetane as intermediate in the formation of the carbon-carbon double bond (Scheme 1).¹ In a seminal article published in 1953, Wittig and Geissler also proposed the participation of a 1,2-oxaphosphetane in the synthesis of 1,1-diphenylethylene by reacting $\text{Ph}_3\text{P}=\text{CH}_2$ with benzophenone.² This work represents the birth of the olefination of aldehydes and ketones by phosphorus ylides, the Wittig reaction, which evolved into a reference synthetic method for the regio- and stereodefined construction of carbon-carbon double bonds.^{3,4} Despite being intensively studied for almost 70 years, the mechanism of this fundamental transformation in organic synthesis is still under debate. In an excellent recent review, Gilheany and Byrne performed a detailed analysis of the experimental and computational studies about the mechanism of the Wittig reaction between phosphonium ylides and aldehydes or ketones.⁵ Phosphorus ylides are categorized by the substituent(s) R attached to the ylidic carbon as non-stabilized (R = alkyl), semi-stabilized (R = alkenyl, phenyl) and stabilized (R = heteroatom-containing conjugating group, e.g., carbonyl, ester, nitrile, etc.). The accepted mechanism for the Li-salt free Wittig olefination of non-stabilized ylides under kinetic control involves a [2+2] cycloaddition to give a 1,2-oxaphosphetane intermediate (*cis*-OPA/*trans*-OPA, Scheme 1), which decomposes via the isomer formed by phosphorus pseudorotation to place the P-O bond in equatorial position (*cis*-OPA_{eq}/*trans*-OPA_{eq}) followed by [2+2] cycloreversion to yield the olefin (*Z*-OL/*E*-OL), and a phosphine oxide (Scheme 1).^{6,7}

In the absence of inorganic salts, the stereochemical course of the process can be explained through a combination of [1,2]-,^{6,8} [1,3]-,⁶ C-H...O,^{4c,9} and dipole-dipole⁹ interactions that control the relative energy of the transition states (*cis*-TS/*trans*-TS) of 1,2-oxaphosphetanes formation

(Scheme 1). In a few cases, reversibility in this first step has been observed and the *E/Z* selectivity obtained proceeds from the thermodynamic equilibrium between the diastereomeric oxaphosphetanes. This reversal of the cycloaddition step causes the so called stereochemical drift.^{10,11}



Scheme 1: Mechanism of Wittig olefination. Stereoelectronic interactions are highlighted in blue.

Hundred years after 1,2-oxaphosphetanes were first introduced,¹ they remain the only intermediates isolated in the Wittig reaction. Experimental evidences about the participation of 1,2-oxaphosphetanes in the Wittig olefination arise mostly from *in situ* NMR monitoring of the process at low temperature.^{10,12,13} Generally, 1,2-oxaphosphetanes are highly thermally labile species and are transformed into the corresponding olefin and P=O by-product upon warming the NMR sample. A very small number of these intermediates have been isolated and structurally characterized through X-ray diffraction studies.¹⁴ Representative examples are shown in Chart 1. Based on the origin of their thermal stability, they can be classified into two groups. Group A is formed by mono-heterocyclic systems stabilized by strong electron-withdrawing substituents (e.g., **1**,¹⁵ **2**,¹⁶ and **3**¹⁷). Group B includes compounds characterized by the integration of the oxaphosphetane moiety into a polycyclic system. Spiro-compounds with rings connected through a pentacoordinated phosphorus atom seem to represent a particularly stable arrangement, as shown by the spiro-oxaphosphetanes **4**,¹⁸ **5**,¹⁹ and **6**.²⁰ The Martin ligand²¹ (ML) and the *ortho*-benzamide ligand (*o*BA) proved to be very efficient scaffolds for OPA stabilization.^{22,23} So far, only 1,2-oxaphosphetanes derived from non-

stabilized ylides have been isolated as products of the Wittig reaction. It is nevertheless important to note that 1,2-oxaphosphetanes formally arising from ylides stabilized by a methoxycarbonyl group have been obtained through alkoxy-carbonylation of stable precursors unsubstituted at C-3 (i.e., proceeding from non-stabilized ylides).²⁴

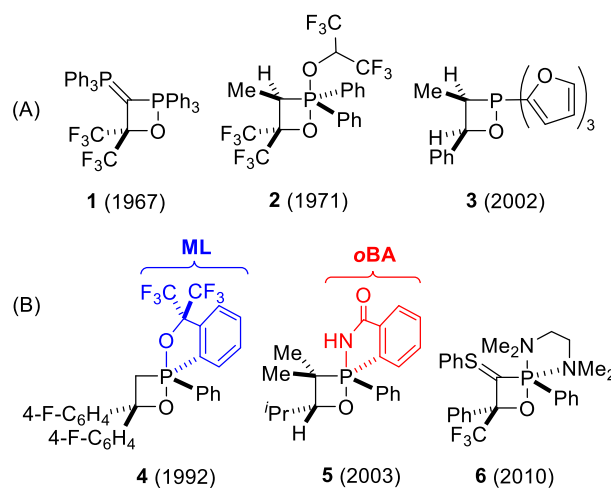
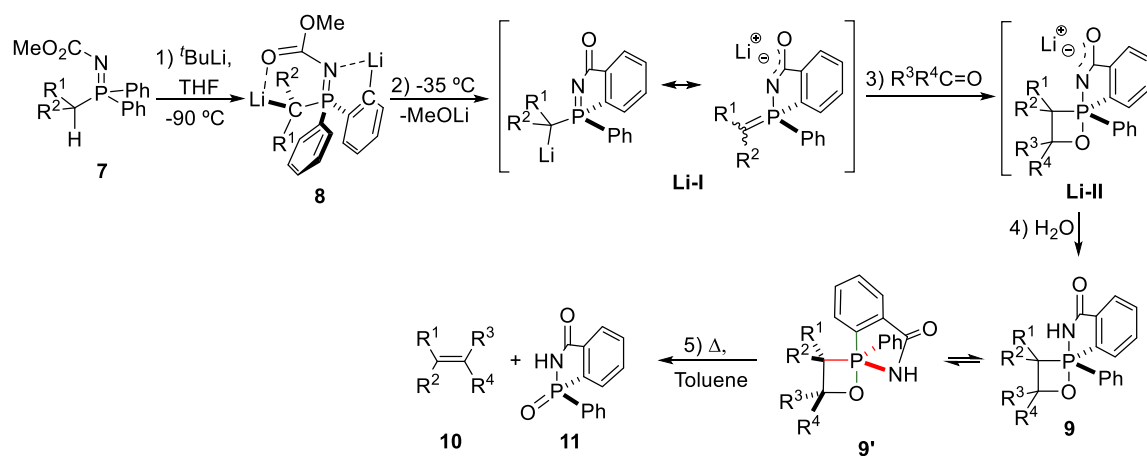


Chart 1. Examples of 1,2-oxaphosphetanes characterized in the solid-state with X-ray diffraction.

Ligands ML and *o*BA are highlighted in blue and red color, respectively.

Although most oxaphosphetanes isolated undergo olefination upon heating, the rather simple substitution pattern prevents gaining insight into the stereoelectronic effects that govern the reaction. We have previously shown that the stabilizing effect of the *o*BA ligand allowed to obtain stable tri- and tetra-substituted spiro-1,2-oxaphosphetanes **9** in an one-pot two-steps process (Scheme 2).^{19,23} Firstly, double C_α and C_{ortho} deprotonation of phosphazene **7** with ^tBuLi at -90 °C provides dianion **8**,²⁵ which undergoes cyclocondensation at -35 °C by attack of the ortho anion to the carbonyl group of the phosphazene moiety followed by elimination of lithium methoxide to give the monoanionic intermediate **Li-I**. Then, reaction of **Li-I** with aldehydes and ketones would afford lithiated species **Li-II**, which is converted into spiro-1,2-oxaphosphetanes **9** upon aqueous workup. The thermolysis of **9** in toluene solution afforded the corresponding olefins **10** in a quantitative and stereospecific manner (Scheme 2).^{19,23} In contrast to the accepted mechanism mentioned above,^{5,26} the computational study of the thermal decomposition of **9** revealed that the [2+2] OPA cycloreversion to the corresponding alkenes **10** and benzoazaphospholone 1-oxide **11** is a single step asynchronous

reaction.²⁷ The positional interchange of apical and equatorial ligands around the phosphorus atom leading to an anti-apicophilic P–O_{eq} OPA takes place along the reaction coordinate via mechanisms involving two (M_{B2}) or three (M_{B3}) and four (M_{B4}) Berry pseudorotations (BPR).²³ These mechanisms also explained the isomerization of OPA **9** into **9'** through inversion of the configuration of the phosphorus atom during thermal decomposition (Scheme 2).



Scheme 2. Synthesis of spiro-1,2-oxaphosphetanes **9** and alkenes **10**.

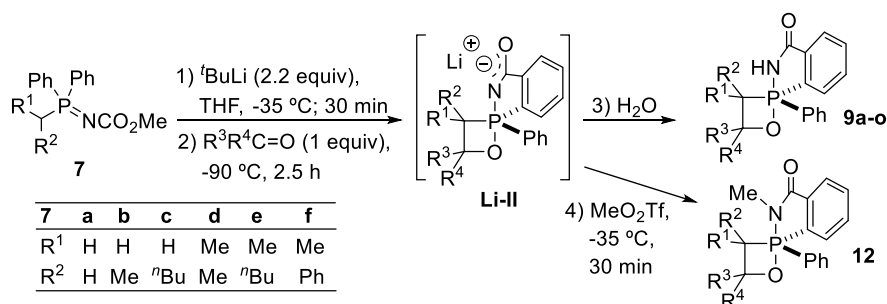
In the light of the stability of spiro-compounds **9**, we reasoned that they could be used for investigating the stereoelectronic features controlling olefin formation in the second step of Wittig olefination. Here we report the extension of the synthesis of *o*BA-stabilized spiro-oxaphosphetanes to the preparation of compounds with a substitution pattern that allows to unraveling the effects determining the course of the olefination process via thermolysis. New developments include the synthesis of *N*-alkylated derivatives and the isolation and structural characterization of the first example of a 1,2-oxaphosphetane derived from a semi-stabilized ylide derivative. Kinetic and thermodynamic parameters obtained in the olefination study revealed the influence of electronic and solvent effects as well as steric [1,2] and, [1,3] interactions in the reaction pathway.

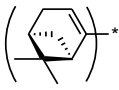
Results and Discussion

Synthesis of *o*BA stabilized spiro-1,2-oxaphosphetanes. Compounds **9** used in this study were prepared according to the procedure shown in Scheme 2 (Table 1).²⁵ Oxaphosphetanes **9a-p** were

1
2 obtained in very high to excellent yields, except for **9p** (see below). High yields of **9e** and **9i** were
3
4 achieved by increasing the reaction time to 5 h (entry 5) and the reaction temperature to -35 °C (entry
5
6
7 **9c**,²³ **9d**,²³ **9e**,²⁵ **9j**,²⁵ and **9l**²⁵ reported previously have been included
8
9 here in order to complete the kinetic studies and the analysis of the effects involved in the Wittig
10
11 olefination. The reactions of phosphazenes **7b-c** monosubstituted at the *P*-C α proceeded with
12
13 excellent diastereoselectivity (c.f. entries 12-15), whereas C α -disubstituted phosphazenes **7d-e**
14
15 provide oxaphosphetanes **9** with moderate to low diastereoselectivity (entries 5, 10 and 11).
16
17 Diastereoisomers were separated by precipitation from diethyl ether or by column chromatography.
18
19 All compounds were structurally characterized based on their spectroscopic data (Supporting
20
21 Information). The stereochemistry was assigned through selective 1D gNOESY experiments.
22
23 Recrystallization of oxaphosphetane *cis*-**9d** from a mixture of dichloromethane-hexane afforded
24
25 single crystals suitable for X-ray diffraction analysis. The crystal structure is shown in Figure S13
26
27 (supporting information). Oxaphosphetanes *cis/trans*-**9k** formed in the reaction of dilithiated **7d** with
28
29 (-)-mirtanal ((-)-(1*S*,5*R*)-6,6-dimethylbicyclo[3.1.1]-2-hepten-2-carbaldehyde) are enantiomerically
30
31 pure. Their configuration were assigned based on the 2D gNOESY spectra. This structural study
32
33 evidenced that the racemic phosphazenylium carbanion added to the carbonyl group of (-)-mirtanal
34
35 exclusively through the *si* face. Isomer *trans*-**9k** was recrystallized from a mixture of
36
37 dichloromethane-hexane and the X-ray crystal structure was measured (Figure S14).
38
39
40
41
42
43

44 The reaction of benzylphosphazene **7f** deserves particular comment (Scheme 3). The phenyl ring
45
46 attached to the P-CH carbon means that this substrate will be the precursor of a semi-stabilized
47
48 phosphorus ylide derivative (species **Li-I** in Scheme 2). Under the reaction conditions shown in Table
49
50 1 and using acetone as carbonyl component, spiro-OPA *cis*- and *trans*-**9p** were obtained with 17%
51
52 conversion together with a large amount of starting material (26%) and a number of by-products
53
54 (57%) (Scheme 3). After some experimentation, we found that the cleanest reaction leading to **9p**
55
56 consisted of performing the double deprotonation in the standard manner followed by addition of 5
57
58 equiv of acetone at -90 °C and allowing the temperature to rise to -35 °C during 90 min.
59
60

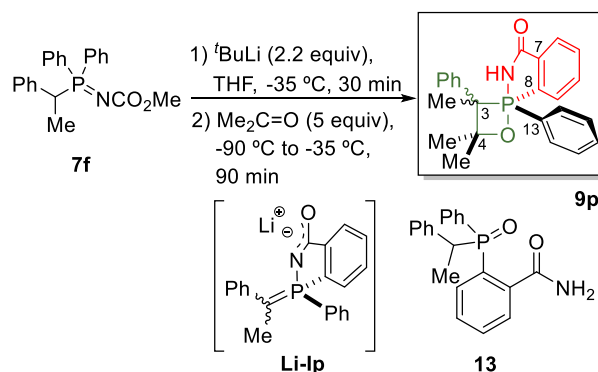
Table 1. Spiro-1,2-oxaphosphetanes **9** and **12** synthesized and ^{31}P NMR data, δ in ppm.

Entry	Comp.	R ¹	R ²	R ³	R ⁴	Trans:cis ^a	Conv. (%)	$\delta(^{31}\text{P})$ Trans/cis ^a
1	9a	Me	Me	Me	Me		92	-63.9
2	9b	Me	Me	CH ₂ (CH ₂) ₃ CH ₂			93	-64.7
3	9c^b	Me	Me	Ph	Ph		92	-65.5
4	9d^b	Me	Me	Me	Ph		92	-65.5
5	9e^c	Me	ⁿ Bu	Me	Ph	76:24	65 (86) ^d	-66.6/-67.0
6	9f	Me	Me	<i>p</i> -F-C ₆ H ₄	<i>p</i> -F-C ₆ H ₄		93	-65.4
7	9g	Me	Me	<i>p</i> -Cl-C ₆ H ₄	<i>p</i> -Cl-C ₆ H ₄		95	-65.4
8	9h	Me	Me	<i>m</i> -CF ₃ -C ₆ H ₄	<i>m</i> -CF ₃ -C ₆ H ₄		97	-65.1
9	9i	Me	Me	<i>p</i> -Me ₂ N-C ₆ H ₄	<i>p</i> -Me ₂ N-C ₆ H ₄		88 ^e	-64.2
10	9j^c	Me	Me	H	<i>p</i> -MeO-C ₆ H ₄	40:60	93	-65.0/-63.9
11	9k	Me	Me	H	() [*]	51:49	96	-63.7/-63.6
12	9l^c	Me	H	CH ₂ (CH ₂) ₃ CH ₂		5:95	82	-70.5/-73.4
13	9m	Me	H	Ph	Ph	3:97	89	-69.5/-72.4
14	9n	ⁿ Bu	H	Me	Ph	0:100	87	-75.9
15	9o	Me	H	<i>p</i> -MeO-C ₆ H ₄	<i>p</i> -MeO-C ₆ H ₄	0:100	83	-72.8
16	9p	Ph	Me	Me	Me	34:66	27	-68.3/-67.5
17	12a	Me	Me	Me	Me		95	-53.4
18	<i>cis</i> - 12b^a	Me	H	Ph	Ph		87	-59.8
19	12c	Me	Me	Ph	Ph		95	-48.9
20	12d	Me	Me	<i>p</i> -MeO-C ₆ H ₄	<i>p</i> -MeO-C ₆ H ₄		91	-48.7

^a) Diastereomeric ratios determined through integration of the ^{31}P NMR spectra of the crude reaction mixture. Trans/cis descriptors indicate the relative orientation of the *P*-phenyl ring and the higher rank substituent linked either to C3 and/or C4 carbons of the oxaphosphetane ring. ^b) Compound described in reference 23. ^c) Compounds described in reference 25. ^d) Reaction time with the ketone of 5 h. ^e) Reaction time with the ketone of 5 h at a temperature of -35 °C.

In this way, oxaphosphetanes *cis*-/*trans*-**9p** were obtained in a conversion of 27% and a ratio of 66:34 (Table 1) together with unreacted **7f** (38%) and the phosphorylbenzamides **13** (35%, mixture of two diastereoisomers in a ratio of 14:21) (Figure S1, Supporting Information). The formation of significant amounts of by-products **13** arising from the hydrolysis of the lithiated cyclization

intermediate **Li-Ip** is in agreement with the suggested reduction in nucleophilic reactivity of **Li-Ip** towards the carbonyl group of acetone.



Scheme 3. Synthesis of spiro-1,2-oxaphosphetane **9p**.

Purification through two consecutive column chromatographies provided a small amount (2.6 mg, yield 1%!) of nearly pure *cis*-**9p**, enough to achieve the structural characterization through mass spectrometry and spectroscopic methods. The HRMS spectrum showed the $[\text{M}+\text{H}]^+$ ion at m/z 390.1639 in agreement with the molecular formula of protonated **9p** ($\text{C}_{24}\text{H}_{25}\text{NO}_2\text{P}$ calculated exact mass: 390.1623). The ^{31}P NMR spectrum shows a resonance at δ -67.5 ppm in the expected range for a pentacoordinated phosphorus atom (Figure S2d). The ^1H and ^{13}C NMR spectra present the same pattern of signals of the family of compounds **9** (Figures S2a and S2c). The relative configuration of the P and C stereogenic centers was established based on 1D NOE experiments (Figure S2b). To the best of our knowledge, this is the first example of an 1,2-oxaphosphetane isolated from a semi-stabilized phosphorus ylide having a phenyl group at the ylidic carbon. It should be noted that Vedejs and Fleck reported the observation through ^{31}P NMR of C3-vinyl substituted OPAs stabilized by a dibenzophosphole system.^{6c}

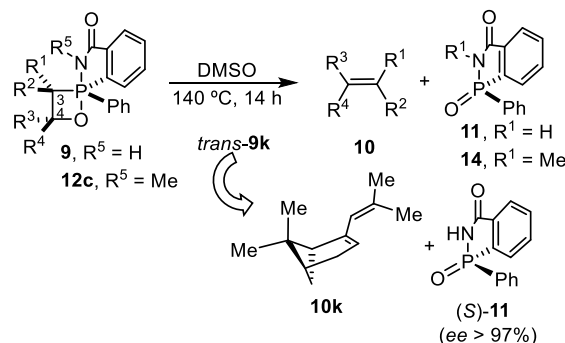
Spiro-oxaphosphetanes **9** contain an N–H bond that might participate in the olefination reaction via hydrogen bonding with the solvent, the phosphorus by-product or through self-association. To eliminate these possible contributions to the olefination process we sought to prepare *N*-methylated derivatives of **9**. Quenching the lithiated species **Li-II** with methyl trifluoromethanesulfonate (MeOTf) at $-35\text{ }^\circ\text{C}$ during 30 min furnished *N*-methyl spiro-oxaphosphetanes **12** in excellent yields (Table 1, entries 17 - 20). *N*-Methylation is evidenced by the ^1H NMR spectra. Recrystallization of

1
2 **12a** from hexane afforded crystal suitable for X-ray diffraction analysis. The structure obtained is
3
4 shown in Figure S15. A brief analysis of the main solid-state structural features of compounds *cis*-
5
6 **9d**, *trans*-**9k**, and **12a** is given in the Supporting Information. The synthesis of **12** illustrates the wide
7
8 scope of the methodology developed for the preparation of spiro-1,2-oxaphosphetanes making
9
10 feasible the derivatization of the spiranic system in a one-pot manner. Furthermore, the *N*-methylated
11
12 *o*BA ligand (MoBA) of **12** introduce new interactions with the substituents at carbon C3 of the
13
14 oxaphosphetane ring, which will be analyzed below.
15
16

17
18 **Synthesis of olefins by thermolysis of spiro-1,2-oxaphosphetanes.** Spiro-1,2-oxaphosphetanes **9**
19
20 undergo a quantitative transformation into the corresponding alkenes **10** and benzazaphospholone **11**
21
22 by heating in DMSO-*d*₆ at 140 °C overnight in a NMR tube (Table 2). *E/Z* isomerization was not
23
24 observed during the NMR monitoring process, i.e., stereochemical drift did not took place. Pure
25
26 alkenes were obtained by dissolving the DMSO solution into CH₂Cl₂, washing with water followed
27
28 by solvent elimination *in vacuo*. Addition of hexane to the crude reaction mixture dissolved the olefin
29
30 and induced the quantitative precipitation of **11**. No signal was detected in the ³¹P NMR spectrum of
31
32 the hexane solution. Finally, solvent evaporation afforded pure tri- and tetra-substituted alkenes **10**.
33
34 The configuration of the carbon-carbon double bond was assigned based on the NOEs detected in 1D
35
36 gNOESY spectra. Changes in the phosphorus configuration²⁸ could be unraveled by investigating the
37
38 olefination of enantiomerically pure compounds *cis*-**9k** and *trans*-**9k** (Table 2). Although their
39
40 thermolysis led to an alkene devoid of geometrical isomers, the benzazaphosphole **11** generated is
41
42 chiral and arises from an enantiomerically pure oxaphosphetane with a phosphorus atom of (*R*) and
43
44 (*S*) configuration, respectively.²⁹ Heating *cis*-**9k** at 130 °C in DMSO during 6 h afforded **10k** and **11**
45
46 quantitatively. Chiral HPLC analysis of **11** showed an enantiomeric ratio (*R*)-**11**:(*S*)-**11** of 76:24
47
48 (Figure S3, based on the known absolute configuration of (*S*)-**11**).²³ Clearly, stereomutation occurred
49
50 during fragmentation of the oxaphosphetane ring, causing partial racemization of **11**. This P-
51
52 isomerization during olefination has been previously ascertained in *o*BA-stabilized OPAs.²³
53
54 Interestingly, the analogous reaction of *trans*-**9k** provided enantiomerically pure **11** (Figure S3). This
55
56
57
58
59
60

means that for this isomer the reaction takes place stereospecifically without apparent stereomutation of the phosphorus atom.

Table 2. Alkenes **10** obtained by thermolysis of oxaphosphetanes **9** and **12c**.^a



Entry	9	10	R ¹	R ²	R ³	R ⁴
1	a	a	Me	Me	Me	Me
2	b	b	Me	Me	CH ₂ (CH ₂) ₃ CH ₂	
3	c	c^b	Me	Me	Ph	Ph
4	<i>cis-d</i>	d	Me	Me	Me	Ph
5	<i>trans-e</i>	<i>E-e</i>	ⁿ Bu	Me	Me	Ph
6	<i>cis-e</i>	<i>Z-e</i>	Me	ⁿ Bu	Me	Ph
7	<i>trans-j</i>	j	Me	Me	H	<i>p</i> -MeO-C ₆ H ₄
8	<i>trans-k/cis-k</i>	k	Me	Me	H	
9	<i>cis-l</i>	l	H	Me	CH ₂ (CH ₂) ₃ CH ₂	
10	<i>cis-m</i>	m	H	Me	Ph	Ph
11	<i>cis-n</i>	<i>Z-n</i>	H	ⁿ Bu	Me	Ph
12	<i>cis-o</i>	o	H	Me	<i>p</i> -MeO-C ₆ H ₄	<i>p</i> -MeO-C ₆ H ₄
13	<i>cis-p</i>	d	Me	Ph	Me	Me

^a) Alkenes have been labeled with the same alphabetical identifier of the oxaphosphetane precursor. ^b) The same alkene is formed in the thermolysis of **12c**.

The thermal decomposition of the *N*-methylated oxaphosphosphetane **12c** proceeded in an analogous manner to that of compounds **9** affording alkene **10c** and *N*-methyl benzazaphospholone **14** quantitatively.

Kinetic study of the thermolysis of spiro-1,2-oxaphosphetanes. To gain insight into the factors determining the energy profile of the second step of the Wittig reaction, we carried out a kinetic study of the thermolytic fragmentation of **9/12c**. The study was aimed at establishing relationships among the factors contributing to the relative stability of the ground state (GS) and transition state (TS) of the olefination with kinetic and thermodynamic data of the transformation. The substituents in the compounds selected may influence the reaction course through electronic effects, [1,2]/[1,3] steric interactions, and hydrogen bonding. Solvent effects were evaluated by measuring olefination rates in DMSO, DMF and toluene. These effects are indicated using a color key in Chart 2. The TS shown in Chart 2 is that considered more representative of the olefination reaction (see computational section).^{5,9,23}

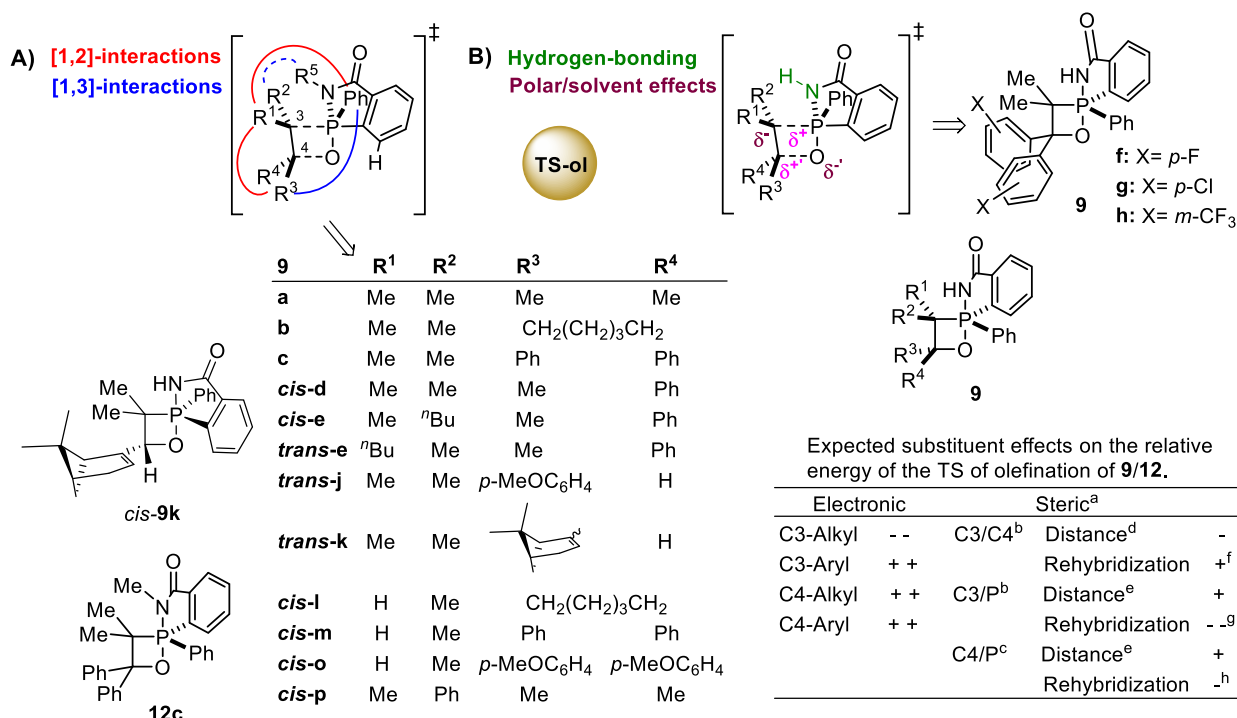


Chart 2. Spiro-1,2-oxaphosphetanes selected for thermal decomposition studies. Stabilization or destabilization of TS is indicated by a + or - sign, respectively. ^{a)} As compared with the GS. ^{b)} [1,2] Interactions. ^{c)} [1,3] Interactions. ^{d)} Decrease in the TS. ^{e)} Increase in the TS. ^{f)} Distance between substituents is expected to increase. ^{g)} Substituents eclipsed. ^{h)} Distance between substituents is expected to decrease.

[1,2] Interactions may be observed between C3/C4 and C3/P substituents. The asymmetric phosphorus atom of **9/12c** would lead to two different C3/P-[1,2] interactions labeled as C3/P_N-[1,2] and C3/P_{Ph}-[1,2]. The subscript designates the P-group syn to a C3 substituent. Substituents in C4/P would give rise to [1,3] interactions. A distinguishing feature of compounds **9/12c** is the much higher thermal stability as compared with 1,2-oxaphosphetanes generated in standard Wittig processes. Since substituents in C3 and C4 of **9/12c** are commonly found in Wittig reactions, their stability, i.e., the difficulty of olefination, must arise from the destabilization of the TS produced by spiranization. Taking into account that the consensus mechanism of olefination involves stereomutation of the phosphorus atom, the TS of the formation of alkenes **10** will be destabilized by three effects: the presence of two electronegative substituents in equatorial sites of a trigonal bipyramidal phosphorus (tbp, antiapicophilic element effect), the ring constrains arising from the five-membered ring (ring effect distortion of tbp), and the steric interaction generated by the NR⁵ moiety eclipsed with one substituent in C3. These features make the decomposition of spiro-oxaphosphetanes **9/12c** the rate determining step in the synthesis of alkenes **10**.

The kinetic of olefination was monitored through ³¹P NMR spectroscopy. A known amount of **9/12c** was heated in the selected solvent and ³¹P NMR spectra were acquired at set time intervals. Monitoring the integrals of the upfield signal typical of oxaphosphetanes **9/12c** (δ in the range -65 to -75 ppm) and the peak at δ 20.5 ppm corresponding to **11** (in DMSO-*d*₆), afforded the concentration of each species as a function of time. The reaction showed a first order dependence in the oxaphosphetane, as established by standard methods. The rate constants measured are summarized in Table 3 (for details see Table S1). The error associated with the measurement of *k* is considered to be $\leq 2\%$.³⁰

Rate differences will be determined by the balance of electronic and steric effects in the TS in the spiranic system. An overview of these effects is given in Chart 2. Based on atom electronegativities C3 and C4 atoms in **9/12c** will bear a negative and positive partial charge, respectively, in the GS.

Table 3. Rate constants for thermal decomposition of oxaphosphetanes shown in Chart 2.

Entry	Compound	k (s^{-1})			T ($^{\circ}C$)
		DMSO- d_6	Toluene- d_8	DMF- d_7	
1	9a		$3.75(3) \times 10^{-4}$		140
			$1.57(2) \times 10^{-4}$		130
2	9b		$6.10(12) \times 10^{-4}$		140
			$2.9(6) \times 10^{-4}$		130
3	9c		$0.98(2) \times 10^{-4}$	$(3.82 \times 10^{-4})^a$	140
			$4.05(8) \times 10^{-5b}$		130
4	cis-9d		$1.80(4) \times 10^{-5}$		130
5	cis-9e		$3.68(7) \times 10^{-5}$		130
6	trans-9e		$7.13(14) \times 10^{-5}$		130
7	cis-9l		$1.85(4) \times 10^{-4}$	$7.80(16) \times 10^{-4}$	70
8	cis-9m		$8.77(18) \times 10^{-5}$		80
9	cis-9o		$3.87(94) \times 10^{-4}$		80
10	trans-9j		$5.5(6) \times 10^{-5}$	$5.0(1) \times 10^{-6c}$	130
11	cis-9k		$0.70(1) \times 10^{-4}$		130
12	trans-9k		$0.90(2) \times 10^{-4}$		130
13	cis-9p		$2.7(1) \times 10^{-3b}$		130
14	12c		$1.08(2) \times 10^{-4}$	$0.91(2) \times 10^{-4}$	160
			$0.43(1) \times 10^{-5}$		130

^{a)} Calculated from the activation parameters in reference 23. ^{b)} Calculated from the activation parameters. ^{c)} Determined at 110 $^{\circ}C$.

These charges are expected to increase in the TS of olefination due to the rupture of C3–P and C4–O bonds. This implies that electron donating substituents in C3/C4 will destabilize/stabilize more

1
2 the TS than the GS. In the reaction pathway, the hybridization of C3/C4 changes from sp^3 to sp^2 . As
3
4 a result, the C3–C4 bond distance would shorten producing larger [1,2] interactions in the TS. This
5
6 effect may be partially compensated by the increase of bond angles undergone by C3/C4. On the other
7
8 hand, the C3–P bond is larger in the TS. Therefore, the substituents will move away from each other
9
10 contributing to the stabilization of the TS. However, due to phosphorus stereomutation, the C3 and P
11
12 substituents become eclipsed in the TS inducing strong [1,2] interactions. Simultaneously, the
13
14 substituents become eclipsed in the TS inducing strong [1,2] interactions. Simultaneously, the
15
16 reordering of C3 and P substituents in the TS approach those linked to C3 and N which gives rise to
17
18 large destabilizing [1,2] interactions. [1,3] Steric effect between C4/P substituents also arises from
19
20 two opposite contributions. Crowding will be relieved in the TS through the increase of the distance
21
22 between these atoms, whereas the C4/P geometrical reordering would destabilize the TS by slightly
23
24 approaching the respective substituents. In the following, a qualitative analysis aimed at identifying
25
26 major contributions to the rate of olefination of compounds shown in Table 3 is provided. Spiro-
27
28 oxaphosphetanes **9/12** can be clustered in three groups according to the number and position of the
29
30 substituents in the four-membered ring. With the exception of *cis-9p* (see below), the thermal stability
31
32 increases in the series trisubstituted-C3-H (group I) \ll trisubstituted-C4-H (group II) \approx
33
34 tetrasubstituted (group III). The fact that trisubstituted OPAs showing one proton at carbon C3
35
36 (entries 7, 8 and 9) olefinate significantly faster than those with the proton at carbon C4 (entries 10,
37
38 11, 12) indicates that the thermal stability is primarily determined by C3/P-[1,2] interactions. The
39
40 eclipsed arrangement of the substituents on the C3 and P atoms of the TS of olefination (**TS-ol**) would
41
42 produce an increase of the energy barrier of decomposition. In agreement with this finding, **12c**
43
44 showed the lowest rate of olefination (entry 14). In the **TS-ol**, the *N*-Me group would be very close
45
46 to the neighbor C3-Me substituent leading to very large C3/P-[1,2] steric interactions. Within OPAs
47
48 of group I, the faster olefination of *cis-9o* with respect to *cis-9m* (factor 4.4, entries 8 and 9) may be
49
50 attributed to the stabilizing charge effect of the methoxy groups in **TS-ol-*cis-9o***.³¹ The comparison
51
52 with *cis-9l* is less evident. The restricted mobility of the cyclohexyl moiety would produce less
53
54 C3/C4-[1,2] steric interactions than the C4-aryl groups of the other member of the group. In addition,
55
56
57
58
59
60

1
2 rehybridization of C4 in **TS-ol-cis-9l** would cause a relief of [1,3] diaxial interactions involving the
3
4 C4–O bond. These features, seem to accelerate slightly the olefination of *cis-9l* when compared with
5
6 *cis-9o* (factor 1.15 at 80 °C in DMSO, Supporting Information). Concerning group II, the differences
7
8 in the rate of olefination of *cis-9k* and *trans-9k* reveal changes in C4/P-[1,3] interactions (entries 11,
9
10 12). The thermolysis of the trans isomer proceeded 1.28 times faster than the cis derivative, which
11
12 suggests that the *P*-phenyl substituent gives rise to larger [1,3] steric hindrance than the *o*BA moiety
13
14 thus destabilizing the TS of *cis-9k* with respect to *trans-9k*.
15
16
17
18

19 OPAs of group III that differ in the substitution pattern at C3 include *cis-9d*, *cis-9e* and *trans-9e*
20
21 (entries 4, 5 and 6). The olefination of *trans-9e* 1.94 times faster than its C3-epimer *cis-9e* (Table 3,
22
23 entries 5, 6) reflects the larger destabilization of **TS-ol-cis-9e** due to stronger C3/C4- and C3/P-[1,2]
24
25 interactions, i.e., [1,2] steric hindrance arising from the *P*-phenyl substituent is also larger than that
26
27 of *o*BA. *cis-9d* underwent the slowest decomposition in this subgroup (2.04 times slower than *cis-*
28
29 *9e*) which points to larger C3/C4- and C3/P-[1,2] steric strain in **TS-ol-cis-9d** compared with the *9e*
30
31 derivatives. The rates of olefination of OPAs of group III bearing different substituents at C4 increase
32
33 in the series *cis-9d* < *9c* < *9a* < *9b* (entries 1-4). These results show that the change of alkyl groups
34
35 at C4 by phenyl substituents increases the energy barrier of olefination. This implies that destabilizing
36
37 steric [1,2]- and [1,3] steric interactions in **TS-ol** of *9c* and *cis-9d* outweigh the electronic stabilization
38
39 provided by the phenyl rings. Differences between *cis-9d/9c* and *9a/9b* can be ascribed to better
40
41 charge delocalization in **TS-ol-9c** and to lower steric hindrance of the cyclohexyl ring compared with
42
43 two methyl substituents (see above), respectively.
44
45
46
47
48

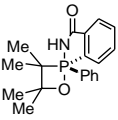
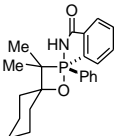
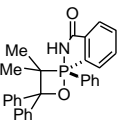
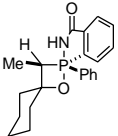
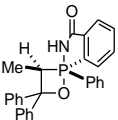
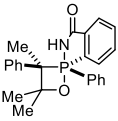
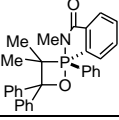
49 The fastest olefination is observed for *cis-9p* (entry 13). The decrease of C3/C4-[1,2] involving
50
51 the C3-phenyl ring of **TS-ol-cis-9p** owing to the increase of distances with the nearby substituents,
52
53 together with the delocalization of the negative charge developed on C3 (Chart 2) will promote a
54
55 large stabilization of the **TS-ol** of *cis-9p*. The easy decomposition of *cis-9p*, an OPA derived from a
56
57 semi-stabilized phosphorus ylide, allows to understand the difficulty in isolating this type of Wittig
58
59 intermediates and the important stabilizing effect of the *o*BA ligand.
60

1
2 To summarize, in absence of C3-aryl substituents large C3/P-[1,2] steric interactions determine
3 the high stability of spiro-oxaphosphetanes. The *P*-phenyl substituent gives rise to larger [1,2] and
4 [1,3] steric hindrance than the *o*BA moiety. Charge delocalization at C4 stabilize the TS of olefination
5 although less efficiently than the destabilization caused by [1,2] and [1,3] steric interactions. In *cis*-
6 **9p** the phenyl group at C3 makes that both steric and electronic effects would contribute to the
7 stabilization of **TS-ol** favoring a large decrease of the barrier of olefination.
8
9
10
11
12
13
14
15

16 The kinetic measurements for representative members of tri- and tetra-substituted spiro-
17 oxaphosphetanes have been performed at different temperatures and the graphic representation of
18 $\ln(k/T)$ as a function of $(1/T)$ (Eyring plot) afforded straight lines from which the activation
19 parameters ΔH^\ddagger and ΔS^\ddagger were calculated (Table 4). Using these values, the Gibbs free energy of
20 activation ΔG^\ddagger for each reaction at a given temperature was calculated. Interestingly, the process
21 involves predominant negative entropic contributions both in the tri- and tetra-substituted series of
22 OPAs and ΔG^\ddagger increases in the series: *cis*-**9l** < *cis*-**9m** < *cis*-**9p** < **9b** < **9a** < **9c** < **12c**. The data
23 collected in Table 4 allow for establishing the dominant role of C3/P_{Ph}-[1,2] interactions over other
24 steric effects in the Wittig olefination of spiranes **9/12**.
25
26
27
28
29
30
31
32
33
34
35
36

37 The ΔG^\ddagger values of compounds dimethylated in C3 are 3.8 – 4.4 kcal·mol⁻¹ larger than those of
38 C3-monomethylated analogues, c.f. **9b/cis-9l**, **9c/cis-9m** (entries 2/4 and 3/5). This $\Delta\Delta G^\ddagger$ represents
39 roughly the contribution to the activation energy of olefination of a C3-methyl group cis to the *o*BA
40 ligand. The difference of 0.6 kcal·mol⁻¹ between the two values can be assigned to slight differences
41 in the steric demand (C3/C4-[1,2] C4/P-[1,3]) of the pentamethylene moiety and the phenyl rings
42 linked to C4. In contrast, changes in ΔG^\ddagger involving C3/C4-[1,2] and C4/P-[1,3]-interactions are in
43 the range of 0.5 – 1.6 kcal·mol⁻¹ (c.f. **9a/9b**, **9a/9c** and **9b/9c**).
44
45
46
47
48
49
50
51
52
53
54
55
56
57
58
59
60

Table 4. Activation parameters of selected spiro-oxaphosphetanes in DMSO-*d*₆.

Entry	Comp	ΔH^\ddagger (kcal·mol ⁻¹)	ΔS^\ddagger (e.u.)	$\Delta G^\ddagger_{403.15\text{ K}}$ (kcal·mol ⁻¹)
1	9a 	30.3 ± 0.5	-1.5 ± 1.2	30.9 ± 1.0
2	9b 	28.5 ± 1.3	-4.7 ± 3.1	30.4 ± 2.5
3	9c 	29.2 ± 1.7	-6.8 ± 4.0	32.0 ± 3.3
4	<i>cis</i> - 9l 	23.1 ± 1.5	-8.8 ± 4.3	26.6 ± 3.2
5	<i>cis</i> - 9m 	25.7 ± 0.1	-4.7 ± 0.2	27.6 ± 0.1
6	<i>cis</i> - 9p 	30.0 ± 3.6	3.7 ± 6.9	28.6 ± 6.3
7	12c 	36.4 ± 1.3	6.8 ± 3.1	33.7 ± 2.6

It must be remembered that an estimation of the role of C3/C4-[1,2] interactions in the decomposition process is complicated by the participation of opposed effects (Chart 2). In particular, elucidating the contribution to the energy of the TS associated to approaching/moving away the substituent in C3 and C4 due to the change of hybridization of these carbon atoms must await to the computational section. The contribution to ΔG^\ddagger of C3/P_N-[1,2] interactions can be quantified by comparing the values of **9a** and **12c** (entries 1, 7). *N*-Methylation produced an increase of 1.72 kcal·mol⁻¹ of the activation energy barrier. Importantly, this larger ΔG^\ddagger of **12c** arises from an increase of the enthalpy of the reaction and a change in the sign of entropic contributions. The latter are now

1
2 positive. Positive entropic effects are also responsible of the lower energy barrier of *cis-9p* with
3
4 respect to **9a** ($\Delta\Delta G^\ddagger = 2.3 \text{ kcal}\cdot\text{mol}^{-1}$).
5
6

7 *Solvent effects.* Solvent may influence the decomposition of **9** and **12** via polar and hydrogen-
8
9 bonding interactions. These features were analyzed by measuring the rate of olefination of **9b**, **9c**,
10
11 *cis-9l*, *trans-9j* and **12c** in DMSO ($\epsilon = 46.45$), DMF ($\epsilon = 36.71$), and toluene ($\epsilon = 2.38$) (Table 3, the
12
13 kinetic study of **9c** in toluene has been previously reported²³). Compounds **9c**,²³ *cis-9l* and *trans-9j*
14
15 olefinated significantly faster in the non-polar solvent toluene than in the most polar solvent of the
16
17 series, DMSO (entries 3, 7 and 10). A similar trend was observed for the rate of olefination of **9b** in
18
19 DMF and DMSO. The reaction in the less polar solvent DMF took place at a slightly higher rate
20
21 (factor 1.15, entry 2). The use of DMSO as solvent increased ΔG^\ddagger of the thermolysis of **9c** in 1.1
22
23 kcal·mol⁻¹ with respect to the reaction reported in toluene (Table 4, entry 3).²³ Both ΔH^\ddagger and ΔS^\ddagger are
24
25 lower in DMSO than in toluene. These results are consistent with a reaction whose TS is more polar
26
27 than the GS. In this situation, the TS will be less efficiently solvated by toluene than by DMSO
28
29 molecules (higher ΔH^\ddagger) and will be less ordered (ΔS^\ddagger more positive). The lower ΔG^\ddagger value for the
30
31 reaction in toluene would reflect the larger contribution of entropic factors to the process.
32
33
34
35
36

37 DMSO may affect the rate of olefination via polar and hydrogen-bonding interactions. The latter
38
39 contribution will be absent in the thermolysis of **12c** lacking the NH group. In this case, olefination
40
41 in DMSO proceeded 1.19 times faster than in DMF (Table 3, entry 14). This behavior can be
42
43 explained by considering that in the absence of hydrogen-bonding, the stabilization on the polar TS
44
45 provided by the more polar solvent (decrease of ΔH^\ddagger) will prevail over the entropic contributions due
46
47 to less efficient solvation.
48
49
50

51 *Stereomutation.* Thermolysis of *cis-9e* and *trans-9e* provided the corresponding olefin together
52
53 with a new spiro-oxaphosphetane (Figure S6). The products obtained *cis-9e''* and *trans-9e''* are
54
55 shown in Chart 3. Full details about the evolution of reaction products as a function of time are given
56
57 in Table S2. A similar finding was observed previously for compounds *cis-9d* and *cis-9l*.²³
58
59
60

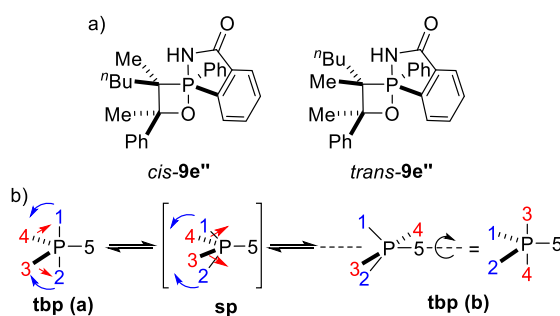


Chart 3. (a) Oxaphosphetanes formed by stereomutation and (b) mechanism of Berry pseudorotation.

The new compounds were identified *in situ* through NMR spectroscopic analysis as permutational isomers in which the configuration of the phosphorus atom is inverted with respect to the starting substrate. The relative configuration was established based on 1D gNOESY spectra (Figure S7). The highest amount of *P*-stereoisomers were obtained for the ratios *cis-9e*:*cis-9e''* of 34.8:21.7 and *trans-9e*:*trans-9e''* of 28.2:9.1, (Table S2). Importantly, the alkenes *Z-10e* and *E-10e* were obtained without traces of products of geometrical isomerization being detected. The retention of the C3/C4 configuration during thermolysis confirms that the new oxaphosphetane formed must be an epimer of the starting compound at the phosphorus center.

Spiro-oxaphosphetanes **9** contain a pentacoordinated phosphorus atom with a tbp geometry. Isomerization may occur through sequential Berry pseudorotations³² (MB1, MB2, MB3, MB4).^{23,33} The process can be visualized in Chart 3 for a tbp with five different ligands. Defining ligand 5 as pivotal center, the angle between apical positions 1 and 2 closes down with simultaneous opening up of the angle involving ligands 3 and 4. In this way, tbp (a) apparently rotates (pseudorotate) toward tbp (b) via a square pyramide (sp) intermediate.

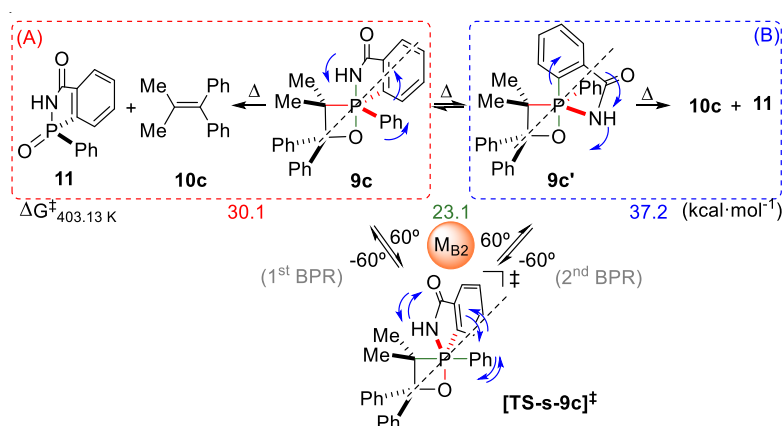
Stereomutation in enantiomerically pure *cis-9k*, implies that the by-product **11** formed in the olefination reaction will be partially racemized. Moreover, the rates of olefination measured do not correspond to a single process. For the determination of the rate constants we have considered that both isomers represent a single reagent. This assumption is compatible with two premises: the two pseudorotamers decompose through a common intermediate (Curtin-Hammett principle) or olefination proceeds through different intermediates of similar activation energies affording average

1
2 rate constants. Support for this latter assumption is provided by the relatively low concentration of
3
4 permutational isomers detected and by the fact that fragmentation of *cis*-**9l** (70 °C), *cis*-**9e** (115 °C),
5
6 and *trans*-**9e** (115 °C) in toluene took place without formation of pseudorotamers. In all cases, the
7
8 representation of $\ln[\mathbf{9}]_t$ against time originates straight lines of $r \geq 0.997$ (Supporting Information).
9
10 The ^{31}P NMR monitoring of the olefination reactions showed that isomerization occurred in parallel
11
12 with olefin formation (Figure S6, Table S2). Considering that stereomutation has been observed in
13
14 most cases in which a new diastereoisomer could be formed, it is reasonable to assume that
15
16 decomposition of spiro-oxaphosphetanes **9** at 130 °C involves, most probably, small contributions of
17
18 phosphorus isomerization processes exchanging the positions of the two equatorial ligands.
19
20
21

22
23 **Computational study of the olefination of spiro-oxaphosphetanes.** The results discussed above
24
25 have revealed that the thermal decomposition of compounds **9** is a process characterized by a negative
26
27 entropy, except for *cis*-**9p** and **12c**, and a polar transition state which relative energy depends on a
28
29 combination of electronic, steric and solvent effects. Besides fragmentation, the pentacoordinated
30
31 phosphorus undergoes stereomutation causing partial racemization of the phosphorus center of some
32
33 derivatives. In order to understand the stereoelectronic factors determining the olefination of spiro-
34
35 oxaphosphetanes we have performed a DFT study of the potential energy surface (PES) for the
36
37 thermolysis of **9** and **12**. Three functionals were evaluated using the olefination of **9a** and **12c** as test
38
39 reactions: B3LYP/6-31G*, M06/6-31G* and M06-L/6-31G* M06-2X/6-31G*. The best results
40
41 including London dispersion correction were obtained with M06-L/6-31G* (Tables S3 and S4) and,
42
43 therefore, this level of theory was applied to all calculations.³⁴ All the stationary points located were
44
45 characterized by computing the harmonic vibrational frequencies. In the case of the transition
46
47 structures, the intrinsic reaction coordinate (IRC) calculations were performed in order to correlate
48
49 the structures found with those of the starting reagents and the reaction products. The computations
50
51 were carried out with the Gaussian09 program.³⁵ Firstly, we completed the study of the
52
53 thermochemistry of **9c** by computing the effect produced by changing the solvent of the
54
55 decomposition reaction from toluene to DMSO. Next, the potential energy surface (PES) of the
56
57
58
59
60

thermolysis of **12c** was investigated with the aim of explaining the higher stability of OPAs bearing the MoBA ligand with respect to the *o*BA-stabilized derivatives. Then, [1,2] and [1,3] interactions were examined by calculating the energy profile of suitably substituted compounds **9** including **9a**, **9b**, **9c**, *cis*-**9m** and **12c**.

We have previously shown that the thermal transformation of **9c** into alkene **10c** and benzoazaphosphole **11** could take place through two mechanisms, A and B (Scheme 4).²³ Route A is the direct conversion of **9c** into products with an activation barrier of 30.1 kcal·mol⁻¹ (recalculated from B3LYP/6-31G* to the level of theory M06-L/6-31G*, Table S5, Figure S8) in excellent agreement with the experimental value of 30.9 kcal·mol⁻¹ determined in toluene as solvent.²³ The formation of **9c** is a highly exothermic and irreversible reaction.



Scheme 4. Key computational results of the olefination of **9c** in the gas phase.

Route B is also a single step process that starts with the permutational isomer **9c'** and proceed to the products through a barrier of 37.2 kcal·mol⁻¹, i.e. decomposition via channel A is highly favored ($\Delta\Delta G^\ddagger = 7.1$ kcal·mol⁻¹). The higher energy barrier of channel B correlates with the larger distortion of the geometry of **TS-ol-9c'** from an ideal tbp, defined by the deviation of the P atom ($\Delta P = 0.228$) from the basal plane,³⁶ with respect to **TS-ol-9c** ($\Delta P = 0.213$) (Figure S8). The anti-apicophilic P-N_{eq} isomer **9c'** is formed by stereomutation of **9c** via a M_{B2} mechanism with a barrier of 23.1 kcal·mol⁻¹. This barrier is 7 kcal·mol⁻¹ lower than the activation energy for olefination via channel A, which indicates that stereomutation of **9c** occurs faster than fragmentation.^{13,28} This feature supports the

1
2 observation of stereoisomers in the olefination of compounds **9** in which inversion of the
3
4 configuration of the phosphorus atom originated a new diastereoisomer (Figure S7).
5

6
7 The single-step mechanism of decomposition of spiro-1,2-oxaphosphetanes **9c** and **9c'** imply that
8
9 the process *does not involve the formation of an intermediate OPA with C3 in apical position*.²⁷
10
11 Analogous results have been found previously in the theoretical study at the MP2 level of the Wittig
12
13 reaction of very simplified model compounds.³⁷ Dynamic calculations on similar systems showed
14
15 that stereomutation takes place almost without energy barrier³⁸ or could not be detected.³⁹
16
17 Furthermore, the TS of olefination is more polar ($\mu = 4.1$ D) than the starting spiro-oxaphosphetane
18
19 ($\mu = 2.97$ D), in agreement with the results of the kinetic study.
20
21
22

23
24 To complete this study, the macroscopic contribution of the solvent to the thermal decomposition
25
26 of **9c** was estimated by using the SMD method of solvent interaction (Table S6).⁴⁰ The ΔG_{solv} obtained
27
28 of 30.0 and 31.6 kcal·mol⁻¹ for the reaction in toluene and DMSO, respectively, are in good agreement
29
30 with those experimentally determined (Tables 3 and 4, entries 3) and support that the decomposition
31
32 of **9c** takes place faster in toluene than in DMSO.
33

34
35 *Theoretical study of the olefination of 12c.* Thermolysis of **12c** is characterized by the largest ΔH^\ddagger
36
37 and ΔS^\ddagger measured, the latter being now positive. Similar to **9c**, the computational study of the
38
39 olefination of **12c** at the M06-L/6-31G* level of theory led to seven stationary points: two spiro-
40
41 oxaphosphetanes isomers, **12c** and **12c'**, the transition states of their stereomutation, **TS-s-12c**, and
42
43 olefination, **TS-ol-12c** and **TS-ol-12c'**, and the reaction products **10c** and **15**. The energy profile is
44
45 shown in Figure 1. Relative energies and thermodynamic parameters are given in Table S7. The
46
47 stationary points located are qualitatively analogue to the corresponding structures calculated for the
48
49 fragmentation of **9c** (Figures S9, S10). **12c** matches the isomer experimentally observed and is
50
51 considerably more stable than the permutational isomer **12c'** ($\Delta\Delta G_{(12c-12c')} = 5.6$ kcal·mol⁻¹ at 130
52
53 °C). This energy difference indicates that the equilibrium between both isomers is completely
54
55 displaced to **12c**, thus explaining that this is the only stereoisomer experimentally observed.
56
57
58
59
60

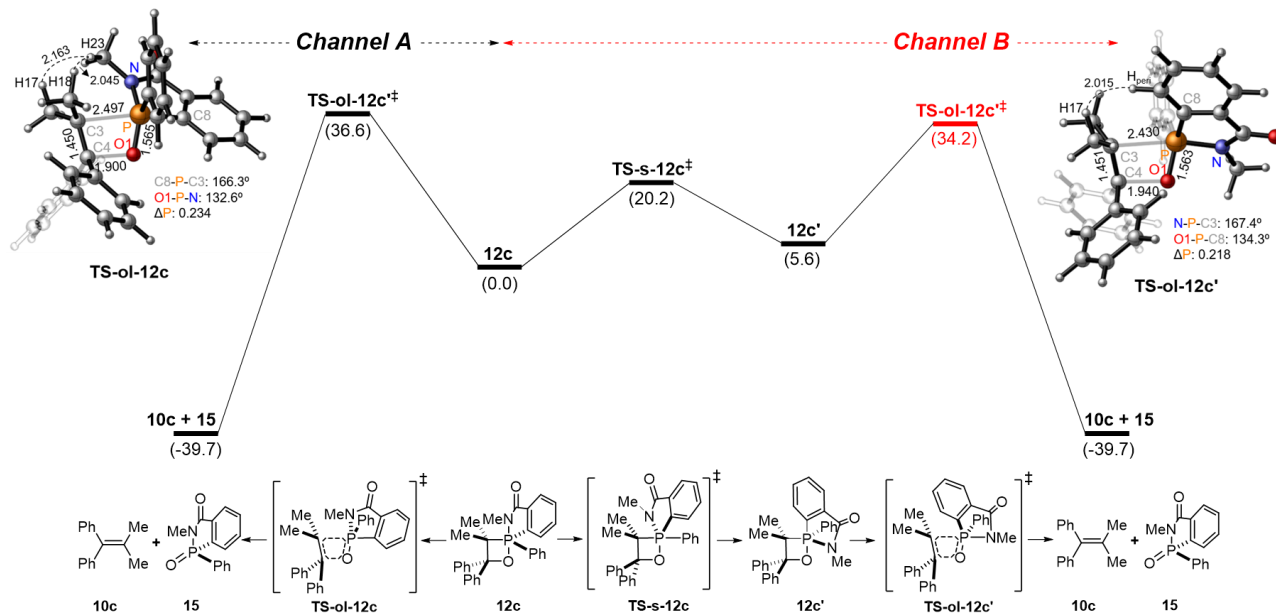


Figure 1. Potential energy surface of the thermal decomposition of **12c** at 130 °C calculated at M06-L/6-31G(d) level of theory. Free energies (in brackets, kcal·mol⁻¹) are relative to the starting materials.

12c/12c' stereomutation proceeds through a M_{B2} mechanism via the transition state **TS-s-12c**. Interestingly, the activation energy barrier of this process (20.2 kcal·mol⁻¹) is 2.9 kcal·mol⁻¹ lower than that calculated for the isomerization of **9c** to **9c'** and significantly lower than the energy required for the olefin-forming reaction. Moreover, the presence of a methyl on the nitrogen shortens the energy gap between isomers **12c** and **12c'** in 0.3 kcal·mol⁻¹ as compared with **9c** and **9c'** (c.f. Tables S5 and S7) and increases the energy liberated in the olefination reaction in 3.6 kcal·mol⁻¹ with respect to **9c**. The higher exothermicity of the decomposition of **12c** is a consequence of the destabilization of its GS with respect to **9c** due to the steric interaction of the N-Me group with the C3-methyl cis to the P-phenyl ring, a structural feature already evidenced in the X-ray structure of **12a** (Figure S15)

Most importantly, contrary to **9c/9c'**, olefination of **12c'** through channel B is energetically favored with respect to **12c** (channel A) by 2.4 kcal·mol⁻¹. This energy difference implies that 95% of the molecules will olefinate via channel B. The destabilization of **TS-ol-12c** arises from the steric hindrance between the methyl groups linked to the nitrogen and to C3 (distortion of the *tbp*, Δ*P* =

0.234, Figure S9). This proximity effect is counterbalanced by a remarkable lengthening of the P–C3 bond distance (2.497 Å, Figure 1). In contrast, the N-Me group of **TS-ol-12c'** is located in a region devoid of relevant steric effects ($\Delta P = 0.218$, Figure S10) and the structural parameters are very similar to those of the TS for the olefination of **9c'**. Therefore, the lower energy barrier calculated for channel B can be assigned to the loss of torsional strain in the transition state as compared with channel A, which correlate with the ΔP values computed. The large positive entropy of activation found for channel B support this hypothesis. Furthermore, the $\Delta G^\ddagger = 34.2 \text{ kcal}\cdot\text{mol}^{-1}$ calculated for olefination through channel B is in good agreement with that experimentally determined in DMSO (Table 4, entry 7). A few anti-apicophilic P–O_{eq} OPAs have been isolated.⁴¹ However, it has been shown that they convert into the P–O_{ap} isomer during thermal decomposition.^{22a}

Analysis of charge effects. Next, we undertook the theoretical study of the stereoelectronic interactions involved in the olefination reaction. Charges distribution around the 1,2-oxaphosphetane ring in the olefination pathway were calculated at the NBO level for derivatives **9a**, **9c** and *cis*-**9m**. The P and O heteroatoms show the expected behavior: higher charges in the transition state than in the ground state (Tables S8). Regarding C3 and C4, the TS of olefination of compounds **9** seems to be stabilized by dispersing the increase of negative/positive charge on C3/C4 through the respective substituents.

Analysis of [1,2] interactions. The calculations above have shown that in the transition state of the olefin-forming step the substituents in carbon C3 and in the phosphorus atom are eclipsed. Therefore, increasing the size of the substituents around the P–C3 bond will destabilize the TS of the reaction. To complement the results obtained for **9c** and **12c**, we have extended the calculations to *cis*-**9m** (Figure S11). The different substitution pattern in C3 of these compounds will allow to correlate differences in the thermodynamic parameters of olefination with steric [1,2] interactions. These may arise from the proximity of the substituents on C3 to those bonded to the phosphorus atom and to C4. Only the most favored pathway of olefination of OPAs stabilized by *o*BA (channel A) and *Mo*BA (channel B) ligands was investigated. Energy parameters and bond distances relevant for the

discussion are given in Table 5. The free energy calculated in the gas phase for the decomposition of *cis-9m* is in excellent agreement with experimental values obtained in the polar solvent DMSO (cf. entries 1/5 of Table 5/4).

Table 5. Calculated (M06-L/6-31G*) energies and activation parameters for the transition states found in the study of [1,2] and [1,3] interactions and selected bond distances in Å.^a

Entry	Structure	ΔE^b	$\Delta H^{\ddagger b}$	$\Delta S^{\ddagger c}$	$\Delta G^{\ddagger b}_{403.15\text{ K}}$	P–C3	C4–O1	C3–C4	P–O1
1	TS-ol-<i>cis-9m</i>	28.9	27.5	0.3	27.4	2.254 (1.838)	1.998 (1.430)	1.428 (1.555)	1.559 (1.777)
2	TS-ol-<i>9c</i>	31.9	30.6	1.3	30.1	2.316 (1.855)	1.975 (1.423)	1.449 (1.576)	1.560 (1.778)
3	TS-ol-<i>9a</i>	30.2	28.7	0.6	28.5	2.362 (1.863)	1.961 (1.438)	1.435 (1.558)	1.556 (1.763)
4	TS-ol-<i>9b</i>	30.0	28.5	0.5	28.3	2.341 (1.85)	1.989 (1.442)	1.436 (1.558)	1.557 (1.761)
5	TS-ol-<i>12c'</i>	36.6	35.2	2.5	34.2	2.430 (1.877)	1.940 (1.424)	1.451 (1.570)	1.563 (1.786)

^{a)} Bond distances in the corresponding OPA ground state are indicated in brackets. ^{b)} The reference structure is indicated by ΔE^{\ddagger} , ΔH^{\ddagger} and $\Delta G^{\ddagger} = 0 \text{ kcal}\cdot\text{mol}^{-1}$. ^{c)} The reference structure is indicated by $\Delta S^{\ddagger} = 0 \text{ e.u. (cal}\cdot\text{K}^{-1}\cdot\text{mol}^{-1})$.

Entries 1, 2 and 5 in Table 5 show some clear trends: (i) the reaction is highly asynchronous (in **TS-ol**, P–C3 and C4–O1 bond dissociations are notably more advanced than C3–C4 and P–O1 double bond formation), (ii) P–C3/C4–O1 bond distances increase/decrease by introducing Me groups at C3 (c.f. **9c** and *cis-9m*, $\Delta_{\text{P-C3}}/\Delta_{\text{C4-O1}} = 0.062/-0.023 \text{ \AA}$) and at the nitrogen atom (c.f. **12c** and **9c**, $\Delta_{\text{P-C3}}/\Delta_{\text{C4-O1}} = 0.114/-0.035 \text{ \AA}$). Therefore, the reaction reaches the **TS-ol** more and more late with increasing number of methyl groups attached to C3 and N. Accordingly, ΔH^{\ddagger} and ΔS^{\ddagger} increase in the series *cis-9m* < **9c** < **12c** (**TS-ol** more product like, increase of disorder). Interestingly, this feature

1
2 correlates with the increment of distortion of the *tbp* from the GS to the TS for the most favored
3
4 olefination channel ($\Delta\Delta P = 0.107$ (*cis*-**9m**, Figure S11), 0.119 (**9c**), 0.149 (**12c**)). The ΔG^\ddagger values
5
6 given in Table 5 indicate that the introduction of a methyl group at C3 produced an increase of the
7
8 energy barrier of olefination of $2.7 \text{ kcal}\cdot\text{mol}^{-1}$. This value is notably smaller than the contribution to
9
10 ΔG^\ddagger of $4.4 \text{ kcal}\cdot\text{mol}^{-1}$ experimentally observed in the polar solvent DMSO (entries 3 and 5, Table 4).
11
12

13
14 The calculations provide support to previous assumptions about the reasons for the stability of
15
16 compounds **9** and the prevailing contribution of C3/P- vs. C3/C4-[1,2] interactions to ΔG^\ddagger . In **TS-ol**
17
18 the C3 and P substituents are eclipsed. The shortest distances are found for the C3-substituent and the
19
20 NH in a mutual *cis* orientation ($2.003/2.007 \text{ \AA}$ for *cis*-**9m/9c**, channel A, Table S9). They are lower
21
22 than the sum of van der Waals radii (2.18 \AA), i.e., along this series **TS-ol** becomes more destabilized
23
24 and ΔG^\ddagger olefination increases, in agreement with the experimental observations. For the *N*-methyl
25
26 derivative **12c**, the strong C3-Me/NMe interactions determined that olefination through channel B
27
28 involving the P-*N*_{eq} isomer **12'** became the preferred pathway of decomposition. During olefination
29
30 substituents in C3 and C4 *cis* to the *P*-phenyl group move away from each other, whereas those *cis*
31
32 to the benzazaphosphole system come closer (Table S9). In any case, the changes in interatomic
33
34 distances are much smaller than those observed for C3/P-[1,2] interactions. Hence, the stability of
35
36 compounds **9/12** can be assigned to strong C3/P-[1,2] interactions in **TS-ol** with those involving the
37
38 NH/NMe being the strongest.
39
40
41
42
43

44
45 C3/C4-[1,2] Interactions are also present, however, they produce two opposing effects and their
46
47 contribution to ΔG^\ddagger of olefination seems to be significantly lower. Although the discussion above has
48
49 been centered on steric effects, it must be remembered that electron-donating groups such as Me at a
50
51 carbon which develops a negative charge in the TS will also contribute to increase ΔG^\ddagger by
52
53 destabilizing **TS-ol**.
54
55

56
57 *Analysis of [1,3] interactions.* The kinetic study of substituents effect in C4 on the rate of
58
59 olefination suggested that large groups in this carbon increased the energy barrier of the reaction due
60
to [1,3] interactions with groups linked to the phosphorus atom. In this context, the contribution of

1
2 the cyclohexyl moiety of **9b** to the rate of decomposition remains arguable. To clarify these
3
4 uncertainties we performed a theoretical study of the olefination of **9a**, **9b** and **9c** having different
5
6 substituents in C4 (Figures S8, S11 and S12). The energies calculated for these transformations and
7
8 some selected bond distances are given in Table 5 (entries 2-4). The olefination barrier increases in
9
10 the series **9b** < **9a** < **9c**, in excellent agreement with the experimental results (Table 4).
11
12

13
14 The analysis of distances of the dissociating/forming bonds in **TS-ol** of the compounds under
15
16 study revealed the existence of only very small differences, insufficient to explain the changes in
17
18 activation parameters shown in Table 5. Differences between **9a** and **9b** can be explained by analyzing
19
20 steric effects between C4/P substituents. The C4-methyl group of cis geometry with the P-phenyl ring
21
22 in the **TS-ol** of **9a** become much closer ($\Delta_{(\text{Me}19\dots\text{PhP})} = -0.423 \text{ \AA}$) than the corresponding C4-CH₂
23
24 protons of the **TS-ol** of **9b** ($\Delta_{(\text{CH}_219\dots\text{PhP})} = -0.136 \text{ \AA}$) (Table S9) causing a larger destabilization of **TS-**
25
26 **ol-9a** with respect to **TS-ol-9b** and, consequently, an increase of ΔG^\ddagger of olefination.
27
28
29

30
31 The replacement of methyl groups by phenyl substituents in C4 (c.f. compounds **9a** and **9c**)
32
33 introduce electronic effects together with [1,2] and [1,3]-interactions. NBO charge calculations
34
35 indicate that the CPh₂ moiety delocalizes the positive charge developed in C4 of **TS-ol** more
36
37 efficiently than the CMe₂ group (Table S8). In the same vein, when going from GS to **TS-ol** of **9c** the
38
39 C4-Ph and P-Ph groups move away (increase of distance of 0.075 Å) leading to less C4/P_{Ph}-[1,3]
40
41 interactions. C3/C4-[1,2] interactions in **TS-ol** of **9a** and **9c** are destabilizing due to the approach of
42
43 the substituents (e.g., change of distances for **9c** between substituents with a cis/trans geometry to the
44
45 *P*-phenyl of -0.072/-0.049 Å). These effects suggest that, contrary to calculations and experimental
46
47 observations, **9c** should olefinate faster than **9a** via a more stabilized **TS-ol**. The key difference
48
49 proceed from the C3/P_{NH}-[1,2] interactions. These are much stronger in **TS-ol-9c** due to a reduction
50
51 of the Me \cdots HN distance of 1.157 Å (vs 0.805 Å for **TS-ol-9a**, Table S9). The destabilization of **TS-**
52
53 **ol** of **9c** caused by this steric effect explains that it shows the largest energy barrier of olefination on
54
55 the series of compounds studied.
56
57
58
59
60

Conclusions

The reaction of C_α,C_{ortho}-dilithiated phosphazenes with aldehydes and ketones represents the first general method of accessing to a large variety of air and temperature stable C3/C4 tri- and tetra-substituted spiro-1,2-oxaphosphetanes stabilized by the *o*BA and MoBA ligands **9/12**. The wide scope of the process is supported by the synthesis of homochiral products using the aldehyde (-)-mirtenal as electrophile and the isolation of the first example of a 1,2-oxaphosphetane derived from a semi-stabilized phosphorus ylide *cis*-**9p**. Stereoselectivities are generally excellent. Mixtures of stereoisomers were readily separated through column chromatography. Their thermolysis afforded the corresponding alkenes quantitatively and stereospecifically. In a number of cases, the permutational isomers by *P*-stereomutation could be structurally characterized *in situ* through NMR spectroscopy. The rates of olefination of **9/12** showed a dependence on stereoelectronic and solvent effects and decreased with increasing number of substituents in C3/C4 and the nitrogen atom. The reaction is characterized by a negative ΔS^\ddagger , except for *N*-methylated derivatives, involved a polar transition state and proceeds faster in low polar solvents.

The computational study of the thermolysis of **9/12** showed that OPAs **9/12** olefinated via species (N, O)(Ph, C₆H₄, C)/(C₆H₄, O)(C, N, Ph) designated as “channel A” and “channel B”, respectively. These processes are associated with the lowest distortion of the *tbp* in the respective TSs. *P*-stereomutation takes place through a M_{B2} mechanism, which exchanged the apical nitrogen with the equatorial C_{ipso} carbon of the *o*BA/MoBA moiety. For both channels, the activation energy of olefination is higher than that of stereomutation. In contrast with the consensus mechanism of Wittig olefination, oxaphosphetane ring fragmentation occurred via a concerted asynchronous reaction (dissociation of P–C3 more advanced than that of C4–O1). The analysis of electronic, solvent and steric effects on the activation energy supported the determining contribution of C3/P-[1,2] interactions to ΔG^\ddagger and the decrease of [1,3]-interactions in the TS of the reaction. This TS is more polar than the starting spiro-oxaphosphetane and showed a distorted *tbp* geometry with C3 and C8 in

apical positions. The higher rate of decomposition observed in solvents of low polarity was a consequence of macroscopic solute-solvent interactions. The stabilization of 1,2-oxaphosphetane through *o*BA and *Mo*BA ligands opens the way to the isolation of elusive intermediate species in the Wittig reaction making feasible their structural and thermochemical characterization. Work is underway to extend the applications of *o*BA and *Mo*BA ligands.

Experimental Section

General information. Melting points were measured on a Büchi B-540 capillary melting point apparatus. High Resolution Mass Spectra were recorded on an Acquity UPLC-Xevo QtoF (Waters) equipment using positive electrospray ionization (ESI). NMR spectra were acquired on a Bruker Avance III HD 300 (^1H 300.13 MHz; ^{13}C 75.47 MHz; ^{19}F 282.40 MHz; ^{31}P 121.49 MHz) and a Bruker Avance III HD 500 (^1H 500.13 MHz; ^{13}C 125.76 MHz; ^{31}P 202.46 MHz) at room temperature using CDCl_3 as solvent. Chemical shifts are referred to internal tetramethylsilane for ^1H and ^{13}C , internal CCl_3F for ^{19}F , and to external 85% H_3PO_4 for ^{31}P . The enantiomeric excesses were determined by HPLC analysis on a HP1100 instrument using Chiralcel OD-H (5 μm , 150 x 4.6 mm) column and a Diode Array detector.

Reactions involving organolithium reagents were performed under an inert atmosphere of nitrogen using Schlenk techniques. Anhydrous solvent were obtained via elution through a solvent column drying system. Commercial reagents were distilled prior to their use, except *t*-BuLi. TLC was performed on Merck plates with aluminum backing and silica gel 60 F₂₅₄. For column chromatography silica gel 60 (40-63 μm) from Scharlau was used. Phosphazenes **7a**,⁴² **7b**,⁴² **7d**⁴³ and **7g**⁴³ (precursor of **7f**) used in this study were prepared according to methods described in the literature. The synthesis of spiro[1,2]-oxaphosphetanes **9c**,²³ **9d**,²⁵ **9e**,²⁵ **9j**,²⁵ and **9l**²⁵ has been reported previously. Compounds **10a** (CAS No. 563-79-1), **10d/10p** (CAS No. 769-57-3), **10l** (CAS No. 1003-64-1), and **10m** (CAS No. 778-66-5) are commercial. Compounds **10b**,⁴⁴ **10c**,⁴⁵ **Z-10e**,^{19,46} **10d** (= **10p**),^{23,47} **E-10e**,^{19,48} **10j**,⁴⁹ **10k**,⁵⁰ **10l**,⁵¹ **Z-10n**,⁴⁸ **10o**,⁵² and **11**¹⁹ have been described previously.

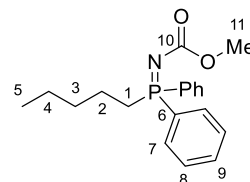
X-ray Crystallographic Studies of *cis*-9d, *trans*-9k, and 12a. A suitable crystal of *cis*-9d, *trans*-9k, and 12a was covered in Paratone-N (Hampton Research) and mounted onto a MiTeGenmicromount. The crystal was transferred directly to a Nonius Kappa CCD diffractometer with CuK α ($\lambda = 1.54184$ Å) for *cis*-9d, an Oxford Diffraction Xcalibur Gemini S with MoK α ($\lambda = 0.71073$ Å) for *trans*-9k and a Bruker Smart 1000 CCD diffractometer with MoK α ($\lambda = 0.71073$ Å) for 12a. The intensities were measured using the oscillation method. The crystal structures were solved by Direct Methods for *cis*-9d and *trans*-9k and Patterson methods for 12a. The refinement was performed using full-matrix least squares on F². All non-H atoms were anisotropically refined. All H atoms were geometrically placed riding on their parent atoms with isotropic displacement parameters set to 1.2 times the U_{eq} of the atoms to which they are attached (1.5 for methyl groups).

Crystallographic calculations were carried out by the X-Ray team, at the University of Oviedo, using the following programs: Collect⁵³ for data collection and HKL Denzo and Scalepack⁵⁴ for cell refinement and data reduction for *cis*-9d ; Bruker SMART⁵⁵ for data collection and cell refinement and Bruker SAINT3⁵⁵ for data reduction for 12a; CrysAlisPro CCD and RES⁵⁶ for data collection, cell refinement and data reduction for *trans*-9k; for structure solution SIR-92⁵⁷ for *cis*-9d, SIR-2004⁵⁸ for *trans*-9k, DIRDIF-2008⁵⁹ for 12a; XABS2⁶⁰ for refined absorption correction; SHELXL-97⁶¹ for structure refinement; WinGX⁶² publication routines and enCIFer⁶³ for preparing material for publication; PLATON⁶⁴ for the geometrical calculations; ORTEP-3⁶⁵ for windows for molecular graphics. Crystal data and structure refinement details for all compounds are outlined on Tables S10-S12. Crystallographic data (excluding structure factors) for the structures reported in this paper have been deposited in The Cambridge Crystallographic Data Centre no. CCDC: 749832 (*cis*-9d), CCDC: 749831 (*trans*-9k), and CCDC: 846036 (12a). These data can be obtained free of charge from the CCDC via <http://www.ccdc.cam.ac.uk/products/csd/request/>.

Computational Methods. Computations were carried out on the Alhambra supercomputer of the IT and Communications Centre (CSIRC) of the University of Granada using the suite of programs Gaussian 09.³⁵ Geometry optimizations, vibrational frequency and natural bond orbital (NBO)⁶⁶

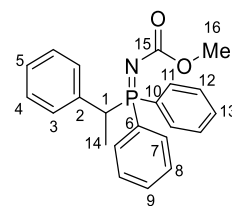
calculations were performed using the M06-L-6-31(d) functional.⁶⁷ All the stationary points located were characterized by performing the harmonic frequency calculations. All minima have zero imaginary frequency, and all transition states have only one imaginary frequency. Intrinsic reaction coordinate (IRC) calculations were performed to establish the connection between ground state, transition state and products.⁶⁸ Single-point energy calculations were carried out using the M06-L functional and basis set 6-311+G(d,p). The SMD⁴⁰ solvation model was used in the single-point energy calculations to incorporate solvent effects with toluene or DMSO as the solvents. Thermal corrections to the Gibbs free energies and enthalpies were calculated using the harmonic oscillator approximation at 403.15 K.

***P*-pentyl-*P,P*-(diphenyl)(*N*-methoxycarbonyl)phosphazene (7c).** Compound **7c** has been synthesized using the same procedure reported for **7a**⁴² and was isolated by precipitation from diethyl ether in a yield of 85%. White solid. Mp 99 - 100 °C.



IR (KBr) ν 1625, 1292 cm^{-1} . ^1H NMR (300.13 MHz, CDCl_3): δ 7.79 (m, 4H, H7), 7.46-7.61 (m, 6H, H8, H9), 3.64 (s, 3H, H11), 2.63 (m, 2H, H1), 1.51 (m, 2H, H2), 1.31 (m, 4H, H3, H4), 0.83 (t, $^3J_{\text{HH}} = 6.9$ Hz, 3H, H5) ppm. $^{13}\text{C}\{^1\text{H}\}$ NMR (75.47 MHz, CDCl_3): δ 162.7 (d, $^2J_{\text{PC}} = 1.7$ Hz, C10), 132.9 (d, $^2J_{\text{PC}} = 9.2$ Hz, C7), 132.2 (d, $^4J_{\text{PC}} = 1.9$ Hz, C9), 128.4 (d, $^3J_{\text{PC}} = 12.1$ Hz, C8), 125.8 (d, $^1J_{\text{PC}} = 93.8$ Hz, C6), 53.5 (d, $^4J_{\text{PC}} = 3.7$ Hz, C11), 29.7 (d, $^3J_{\text{PC}} = 13.0$ Hz, C3), 28.6 (d, $^2J_{\text{PC}} = 1.6$ Hz, C2), 23.0 (d, $^1J_{\text{PC}} = 65.2$ Hz, C1), 13.8 (C5), 22.4 (C4), ppm. $^{31}\text{P}\{^1\text{H}\}$ NMR (121.50 MHz, CDCl_3): δ 25.9 ppm. HRMS (ESI/TOF) m/z : $[\text{M} + 1]$ calcd for $\text{C}_{19}\text{H}_{25}\text{NO}_2\text{P}$, 330.1623; found 330.1638.

Methyl (diphenyl(1-phenylethyl)- λ^5 -phosphanylidene)carbamate (7f). Compound **7f** has been synthesized through α -lithiation of **7g**⁴³ followed by electrophilic quench with methyl iodide using the same procedure reported in the literature for the α -alkylation of phosphazenes.⁴³ **7f** was isolated by precipitation from diethyl ether



in a yield of 66%. White solid. Mp 135-136 °C. IR (KBr) ν 1625, 1311 cm^{-1} . ^1H NMR (300.13 MHz, CDCl_3): δ 7.76 (m, 2H, H11[#]), 7.55 (m, 4H, H7[#], H9, H13), 7.48 (m, 2H, H12^{*}), 7.38 (m, 2H, H8^{*}),

7.16 (m, 3H, H4, H5), 6.92 (m, 2H, H3), 4.51 (dq, $^2J_{\text{PH}} = 15.9$ Hz, $^3J_{\text{HH}} = 7.5$ Hz, 1H, H1), 3.61 (s, 3H, H16), 1.61 (dd, $^3J_{\text{PH}} = 16.9$ Hz, $^3J_{\text{HH}} = 7.5$ Hz, 3H, H14) ppm. $^{13}\text{C}\{^1\text{H}\}$ NMR (75.47 MHz, CDCl_3): δ 162.8 (d, $^2J_{\text{PC}} = 2.4$ Hz, C15), 136.3 (d, $^2J_{\text{PC}} = 5.6$ Hz, C2), 133.3 (d, $^2J_{\text{PC}} = 8.7$ Hz, C11), 133.2 (d, $^2J_{\text{PC}} = 8.7$ Hz, C7), 132.4 (d, $^4J_{\text{PC}} = 2.8$ Hz, C13), 132.2 (d, $^4J_{\text{PC}} = 2.8$ Hz, C9), 128.4 (d, $^3J_{\text{PC}} = 11.6$ Hz, C12), 128.1 (d, $^3J_{\text{PC}} = 11.6$ Hz, C8), 128.1 (d, $^4J_{\text{PC}} = 2.8$ Hz, C4), 127.4 (d, $^5J_{\text{PC}} = 3.3$ Hz, C5), 125.36 (d, $^1J_{\text{PC}} = 95.8$ Hz, C10), 125.3 (d, $^1J_{\text{PC}} = 94.8$ Hz, C6), 52.7 (d, $^4J_{\text{PC}} = 3.7$ Hz, C16), 37.3 (d, $^1J_{\text{PC}} = 58.7$ Hz, C1), 15.6 (d, $^2J_{\text{PC}} = 1.9$ Hz, C14) ppm. $^{31}\text{P}\{^1\text{H}\}$ NMR (121.50 MHz, CDCl_3): δ 29.94 ppm. HRMS (ESI/TOF) m/z : $[\text{M} + 1]$ calcd for $\text{C}_{22}\text{H}_{23}\text{NO}_2\text{P}$, 364.1466; found 330,1478. *.# Interchangeables.

Synthesis. *General procedure for the synthesis of spiro-1,2-oxaphosphetanes 9a-b, f-i, k, m-p.* To a solution of the appropriate phosphazene **7** (6.64×10^{-4} mol) in THF (10 mL) was added a solution of *t*-BuLi (0.86 mL of a 1.7 M solution in cyclohexane, 1.46×10^{-3} mol) at -35 °C. After 30 min of metallation was added the corresponding carbonyl compound (0.66×10^{-3} mol). The reaction mixture was stirred at -95 °C for 2 h 30 min (for the reaction of lithiated **7e/7d** with acetophenone/4,4'-bis(dimethylamino)benzophenone this time was increased to 5 h and 15 h, respectively. In the latter case the temperature used was 35 °C) and then quenched with MeOH. The reaction mixture was poured into water and extracted with dichloromethane (2x15 mL). The organic layers were dried over Na_2SO_4 and concentrated *in vacuo*. ^1H , $^1\text{H}\{^{31}\text{P}\}$, and $^{31}\text{P}\{^1\text{H}\}$ NMR spectra of the crude reaction were always measured in order to determine the stereoselectivity and conversion of the process. The crude mixture was purified by flash column chromatography (eluent: mixture of ethyl acetate:hexane) or by precipitation from diethyl ether to give **9a-p**.

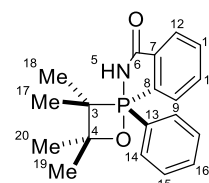
3',3',4',4'-Tetramethyl-1-phenyl-1H-spiro[2,1-benzazaphosphole-1,2'-[1,2]oxaphosphetan]-

3(2H)-one (9a). Conversion 92%. Yield after precipitation from diethyl ether

85%. White solid. Mp 195 - 196 °C. IR (KBr) ν 3435, 3140, 1675 cm^{-1} . ^1H NMR

(300.13 MHz, CDCl_3): δ 8.20 (m, 1H, H9), 8.05 (m, 3H, H12, H14), 7.67 (m, 2H,

H10, H11), 7.41 (m, 3H, H15, H16), 6.43 (d, $^2J_{\text{PH}} = 10.5$ Hz, 1H, H5), 1.45 (d, $^3J_{\text{PH}} = 26.8$ Hz, 3H,



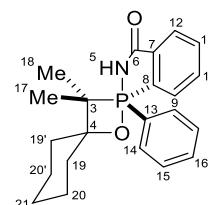
H17), 1.33 (s, 3H, H19), 1.28 (s, 3H, H20), 1.23 (d, $^3J_{\text{PH}} = 26.8$ Hz, 3H, H18) ppm. $^{13}\text{C}\{^1\text{H}\}$ NMR (75.47 MHz, CDCl_3): δ 168.2 (d, $^2J_{\text{PC}} = 4.2$ Hz, C6), 138.2 (d, $^2J_{\text{PC}} = 11.7$ Hz, C7), 136.8 (d, $^1J_{\text{PC}} = 147.8$ Hz, C8), 135.5 (d, $^1J_{\text{PC}} = 142.4$ Hz, C13), 135.5 (d, $^2J_{\text{PC}} = 12.0$ Hz, C9), 134.7 (d, $^2J_{\text{PC}} = 12.0$ Hz, C14), 132.9 (d, $^4J_{\text{PC}} = 3.0$ Hz, C11), 131.9 (d, $^3J_{\text{PC}} = 15.6$ Hz, C10), 131.1 (d, $^4J_{\text{PC}} = 3.6$ Hz, C16), 128.4 (d, $^3J_{\text{PC}} = 15.0$ Hz, C15), 124.4 (d, $^3J_{\text{PC}} = 12.0$ Hz, C12), 72.1 (d, $^2J_{\text{PC}} = 16.2$ Hz, C4), 64.2 (d, $^1J_{\text{PC}} = 109.9$ Hz, C3), 27.0 (d, $^3J_{\text{PC}} = 6.6$ Hz, C20), 26.0 (d, $^3J_{\text{PC}} = 6.6$ Hz, C19), 21.0 (d, $^2J_{\text{PC}} = 6.0$ Hz, C17, C18) ppm. $^{31}\text{P}\{^1\text{H}\}$ NMR (121.50 MHz, CDCl_3): δ -63.9 ppm. HRMS (ESI/TOF) m/z: [M + 1] calcd for $\text{C}_{19}\text{H}_{23}\text{NO}_2\text{P}$, 328.1466; found 328.1469.

3',3'-Dimethyl-1-phenyl-1*H*-dispiro[2,1-benzazaphosphole-1,2'-[1,2]oxaphosphetane-4',1''-

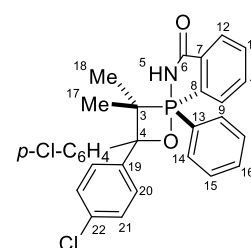
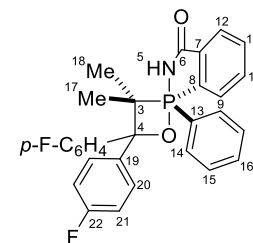
cyclohexan]-3(2*H*)-one (9b). (a = axial, e = equatorial): Conversion 93%. Yield

after precipitation from diethyl ether 87%. White solid. Mp 207-208 °C. IR (KBr)

ν 3430, 1672 cm^{-1} . ^1H NMR (300.13 MHz, CDCl_3): δ 8.25 (m, 1H, H9), 7.97-8.12



(m, 3H, H12, H14), 7.58-7.72 (m, 2H, H10, H11), 7.26-7.41 (m, 3H, H15, H16), 6.23 (d, $^2J_{\text{PH}} = 9.8$ Hz, 1H, H5), 1.57-1.95 (m, 5H, H19_e, H19'_e, H20, H20', H21_e), 1.45 (d, $^3J_{\text{PH}} = 26.8$ Hz, 3H, H17), 1.19 (d, $^3J_{\text{PH}} = 26.8$ Hz, 3H, H18), 1.18-1.38 (m, 3H, H19_a, H19'_a, H21_a) ppm. $^{13}\text{C}\{^1\text{H}\}$ NMR (75.47 MHz, CDCl_3): δ 168.5 (d, $^2J_{\text{PC}} = 4.2$ Hz, C6), 138.3 (d, $^2J_{\text{PC}} = 10.8$ Hz, C7), 137.5 (d, $^1J_{\text{PC}} = 147.2$ Hz, C8), 135.9 (d, $^1J_{\text{PC}} = 142.4$ Hz, C13), 135.3 (d, $^2J_{\text{PC}} = 12.0$ Hz, C9), 135.0 (d, $^2J_{\text{PC}} = 12.0$ Hz, C14), 132.7 (d, $^4J_{\text{PC}} = 3.0$ Hz, C11), 131.7 (d, $^3J_{\text{PC}} = 15.0$ Hz, C10), 131.0 (d, $^4J_{\text{PC}} = 3.0$ Hz, C16), 128.2 (d, $^3J_{\text{PC}} = 14.4$ Hz, C15), 124.2 (d, $^3J_{\text{PC}} = 11.4$ Hz, C12), 72.8 (d, $^2J_{\text{PC}} = 16.2$ Hz, C4), 64.7 (d, $^1J_{\text{PC}} = 108.7$ Hz, C3), 34.9 (d, $^3J_{\text{PC}} = 5.4$ Hz, C19'), 33.9 (d, $^3J_{\text{PC}} = 6.6$ Hz, C19), 25.4 (C21), 22.7 (C20'), 22.6 (C20), 19.8 (d, $^2J_{\text{PC}} = 6.0$ Hz, C17, C18) ppm. $^{31}\text{P}\{^1\text{H}\}$ NMR (121.50 MHz, CDCl_3): δ -64.7 ppm. HRMS (ESI/TOF) m/z: [M + 1] calcd for $\text{C}_{22}\text{H}_{27}\text{NO}_2\text{P}$, 368.1779; found 368.1791.

4',4'-Bis(4-fluorophenyl)-3',3'-dimethyl-1-phenyl-1H-spiro[2,1-benzazaphosphole-1,2'-**[1,2]oxaphosphetan]-3(2H)-one (9f).** Conversion 93%. Yield afterprecipitation from diethyl ether 90%. White solid. Mp 224-227 °C. IR (KBr) ν 3435, 3155, 1672 cm^{-1} . ^1H NMR (500.13 MHz, CDCl_3 , 25 °C) δ 8.69 (dddd, $^3J_{\text{PH}} = 12.7$ Hz, $^3J_{\text{HH}} = 7.5$ Hz, $^4J_{\text{HH}} = 1.2$ Hz, $^5J_{\text{HH}} = 0.5$ Hz, 1H, H9), 8.01(dddd, $^3J_{\text{HH}} = 7.5$ Hz, $^4J_{\text{PH}} = 3.5$ Hz, $^4J_{\text{HH}} = 1.2$ Hz, $^5J_{\text{HH}} = 0.5$ Hz, 1H, H12), 7.81 (tdd, H10, $^3J_{\text{HH}} =$ 7.5 Hz, $^4J_{\text{PH}} = 5.2$ Hz, $^4J_{\text{HH}} = 1.2$ Hz, 1H, H10), 7.69-7.78 (m, 2H, H11 and H14), 7.57 (ddd, $^3J_{\text{HH}} =$ 8.9 Hz, $^4J_{\text{FH}} = 5.3$ Hz, $^4J_{\text{HH}} = 2.7$ Hz, 2H, H20'), 7.31-7.33 (ddd, $^3J_{\text{HH}} = 8.9$ Hz, $^4J_{\text{FH}} = 5.4$ Hz, $^4J_{\text{HH}} =$ 2.7 Hz, 2H, H20), 7.20-7.30 (m, 4H, H5, H15, H16), 6.95 (td, $^3J_{\text{HH}} = ^3J_{\text{FH}} = 8.9$ Hz, $^4J_{\text{HH}} = 2.7$ Hz,2H, H21'), 6.73 (td, $^3J_{\text{HH}} = ^3J_{\text{FH}} = 8.9$ Hz, $^4J_{\text{HH}} = 2.7$ Hz, 2H, H21), 1.66 (d, $^3J_{\text{PH}} = 26.7$ Hz, 3H, H17),1.22 (d, $^3J_{\text{PH}} = 26.5$ Hz, 3H, H18) ppm. $^{13}\text{C}\{^1\text{H}\}$ NMR (125.76 MHz, CDCl_3 , 25 °C) δ 168.1 (d, $^2J_{\text{PC}}$ $= 6.0$ Hz, C6), 161.3 (d, $^1J_{\text{FC}} = 245.4$ Hz, C22), 161.2 (d, $^1J_{\text{FC}} = 245.7$ Hz, C22'), 142.1 (dd, $^3J_{\text{PC}} =$ 11.5 Hz, $^4J_{\text{FC}} = 2.9$ Hz, C19'), 140.3 (t, $^3J_{\text{PC}} = ^4J_{\text{FC}} = 3.1$ Hz, C19), 138.4 (d, $^2J_{\text{PC}} = 10.8$ Hz, C7),136.9 (d, $^1J_{\text{PC}} = 140.8$ Hz, C8), 135.8 (d, $^1J_{\text{PC}} = 152.8$ Hz, C13), 135.4 (d, $^2J_{\text{PC}} = 11.3$ Hz, C9), 133.1(d, $^4J_{\text{PC}} = 2.9$ Hz, C11), 132.2 (d, $^3J_{\text{PC}} = 15.6$ Hz, C10), 131.8 (d, $^2J_{\text{PC}} = 11.0$ Hz, C14), 130.2 (d, $^4J_{\text{PC}}$ $= 3.4$ Hz, C16), 128.6 (d, $^3J_{\text{FC}} = 7.9$ Hz, C20), 128.0 (d, $^3J_{\text{PC}} = 14.6$ Hz, C15), 127.5 (d, $^3J_{\text{FC}} = 7.9$ Hz,C20'), 124.7 (d, $^3J_{\text{PC}} = 12.2$ Hz, C12), 114.7 (d, $^2J_{\text{FC}} = 21.4$ Hz, C21), 114.1 (d, $^2J_{\text{FC}} = 21.1$ Hz, C21'),79.1 (d, $^2J_{\text{PC}} = 13.2$ Hz, C4), 68.2 (d, $^1J_{\text{PC}} = 112.8$ Hz, C3), 23.8 (d, $^2J_{\text{PC}} = 5.0$ Hz, C18), 23.7 (d, $^2J_{\text{PC}}$ $= 4.5$ Hz, C17) ppm. $^{31}\text{P}\{^1\text{H}\}$ NMR (202.46 MHz, CDCl_3 , 25 °C) δ -65.4 ppm. $^{19}\text{F}\{^1\text{H}\}$ NMR (282.40MHz, CDCl_3 , 25 °C) δ -117.4 and -117.1 ppm. HRMS (ESI/TOF) m/z : [M + 1] calcd for $\text{C}_{23}\text{H}_{25}\text{F}_2\text{NO}_2\text{P}$, 488,1591; found 488.1589.**4',4'-Bis(4-chlorophenyl)-3',3'-dimethyl-1-phenyl-1H-spiro[2,1-benzazaphosphole-1,2'-****[1,2]oxaphosphetan]-3(2H)-one (9g).** Conversion 95%. Yield afterprecipitation from diethyl ether 88%. White solid. Mp 214-215 °C. IR (KBr) ν 3415, 3151, 1669 cm^{-1} . ^1H NMR (500.13 MHz, CDCl_3 , 25 °C) δ 8.67 (dddd, $^3J_{\text{PH}} = 12.7$ Hz, $^3J_{\text{HH}} = 7.6$ Hz, $^4J_{\text{HH}} = 1.2$ Hz, $^5J_{\text{HH}} = 0.5$ Hz, 1H, H9), 8.00

(dddd, $^3J_{\text{HH}} = 7.6$ Hz, $^4J_{\text{PH}} = 3.5$ Hz, $^4J_{\text{HH}} = 1.2$ Hz, $^5J_{\text{HH}} = 0.5$ Hz, 1H, H12), 7.53 (dd, $^3J_{\text{HH}} = 8.6$ Hz, $^4J_{\text{HH}} = 2.1$ Hz, 2H, H20'), 7.69-7.84 (m, 4H, H10, H11, H14), 7.21-7.37 (m, 8H, H21', H20, H15, H16, H5), 7.01 (dd, $^3J_{\text{HH}} = 8.7$ Hz, $^4J_{\text{HH}} = 2.3$ Hz, 2H, H21), 1.67 (d, $^3J_{\text{PH}} = 26.7$ Hz, 3H, H17), 1.21 (d, $^3J_{\text{PH}} = 26.6$ Hz, 3H, H18) ppm. $^{13}\text{C}\{^1\text{H}\}$ NMR (75.47 MHz, CDCl_3): δ 168.1 (d, $^2J_{\text{PC}} = 6.2$ Hz, C6), 144.6 (d, $^3J_{\text{PC}} = 11.5$ Hz, C19'), 142.9 (d, $^3J_{\text{PC}} = 3.6$ Hz, C19), 138.3 (d, $^2J_{\text{PC}} = 11.0$ Hz, C7), 136.8 (d, $^1J_{\text{PC}} = 141.3$ Hz, C8), 135.7 (d, $^1J_{\text{PC}} = 152.6$ Hz, C13), 135.4 (d, $^2J_{\text{PC}} = 11.3$ Hz, C9), 133.2 (d, $^4J_{\text{PC}} = 3.1$ Hz, C11), 132.4 (C22), 132.3 (C22'), 132.3 (d, $^3J_{\text{PC}} = 15.1$ Hz, C10), 131.8 (d, $^2J_{\text{PC}} = 11.0$ Hz, C14), 130.3 (d, $^4J_{\text{PC}} = 3.4$ Hz, C16), 128.3 (C21), 128.1 (C21'), 128.0 (d, $^3J_{\text{PC}} = 14.6$ Hz, C15), 127.43 (C20), 127.3 (C20'), 124.7 (d, $^3J_{\text{PC}} = 12.5$ Hz, C12), 79.1 (d, $^2J_{\text{PC}} = 13.0$ Hz, C4), 68.2 (d, $^1J_{\text{PC}} = 113.2$ Hz, C3), 23.7 (d, $^2J_{\text{PC}} = 5.3$ Hz, C18), 23.7 (d, $^2J_{\text{PC}} = 5.3$ Hz, C17) ppm. $^{31}\text{P}\{^1\text{H}\}$ NMR (202.46 MHz, CDCl_3 , 25 °C) δ -65.4 ppm. HRMS (ESI/TOF) m/z : $[\text{M} + 1]$ calcd for $\text{C}_{30}\text{H}_{29}\text{Cl}_2\text{NO}_2\text{P}$, 536.1313; found 536.1328.

4',4'-Bis[3-(trifluoromethyl)phenyl]- 3',3'-dimethyl-1-phenyl-1*H*-spiro[2,1-benzazaphosphole-

1,2'-[1,2]oxaphosphetan]-3(2*H*)-one (9h). Conversion 97%. Yield after precipitation from diethyl ether 89%. White solid. Mp 214-216 °C. IR (KBr)

ν 3473, 1671, 1326, 1166, 1122 cm^{-1} . ^1H NMR (300.13 MHz, CDCl_3): δ 8.78

(dd, $^3J_{\text{PH}} = 12.5$ Hz, $^3J_{\text{HH}} = 7.5$ Hz, 1H, H9), 8.41 (d, $^2J_{\text{PH}} = 10.6$ Hz, 1H, H5),

7.99-8.10 (m, 2H, H12, H20'), 7.80-7.93 (m, 3H, H10, H14), 7.68-7.79 (m, 3H, H11, H22', H24'),

7.57-7.64 (m, 1H, H24), 7.36-7.50 (m, 2H, H20, H23'), 7.15-7.34 (m, 5H, H15, H16, H22, H23), 1.19

(d, $^3J_{\text{PH}} = 26.2$ Hz, 3H, H18), 1.71 (d, $^3J_{\text{PH}} = 26.8$ Hz, 3H, H17) ppm. $^{13}\text{C}\{^1\text{H}\}$ NMR (75.47 MHz,

CDCl_3): δ 168.6 (d, $^2J_{\text{PC}} = 6.7$ Hz, C6), 146.9 (d, $^3J_{\text{PC}} = 11.3$ Hz, C19'), 145.3 (d, $^3J_{\text{PC}} = 3.5$ Hz, C19),

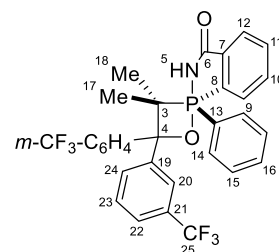
138.4 (d, $^2J_{\text{PC}} = 11.6$ Hz, C7), 136.2 (d, $^1J_{\text{PC}} = 141.0$ Hz, C13), 135.6 (d, $^1J_{\text{PC}} = 152.4$ Hz, C8), 135.4

(d, $^2J_{\text{PC}} = 11.1$ Hz, C9), 133.3 (d, $^4J_{\text{PC}} = 3.0$ Hz, C11), 132.4 (d, $^3J_{\text{PC}} = 15.3$ Hz, C10), 132.0 (d, $^2J_{\text{PC}}$

$= 11.3$ Hz, C14'), 131.8 (d, $^2J_{\text{PC}} = 11.2$ Hz, C14), 130.5 (d, $^4J_{\text{PC}} = 3.5$ Hz, C16), 130.4 (c, $^2J_{\text{FC}} = 32.1$

Hz, C21), 130.2 (c, $^6J_{\text{FC}} = 1.0$ Hz, C24'), 130.0 (c, $^2J_{\text{FC}} = 32.1$ Hz, C21), 129.4 (c, $^6J_{\text{FC}} = 1.2$ Hz, C24),

128.3 (s, C23'), 128.1 (d, $^3J_{\text{PC}} = 14.8$ Hz, C15), 127.7 (s, C23), 124.6 (d, $^3J_{\text{PC}} = 12.3$ Hz, C12), 124.2



(c, $^1J_{FC} = 272.3$ Hz, C25'), 124.0 (c, $^3J_{FC} = 4.0$ Hz, C22'), 123.9 (c, $^1J_{FC} = 272.6$ Hz, C25), 123.5 (c, $^3J_{FC} = 3.6$ Hz, C20'), 123.4 (c, $^3J_{FC} = 3.7$ Hz, C22), 123.0 (c, $^3J_{FC} = 3.9$ Hz, C20), 79.1 (d, $^2J_{PC} = 12.7$ Hz, C4), 68.4 (d, $^1J_{PC} = 113.8$ Hz, C3), 23.5 (d, $^2J_{PC} = 5.1$ Hz, C17, C18) ppm. $^{31}\text{P}\{^1\text{H}\}$ NMR δ (121.50 MHz, CDCl_3): -65.1 ppm. $^{19}\text{F}\{^1\text{H}\}$ NMR (282.4 MHz, CDCl_3): δ -62.6, -62.5 ppm. HRMS (ESI/TOF) m/z: [M + 1] calcd for $\text{C}_{31}\text{H}_{25}\text{F}_6\text{NO}_2\text{P}$, 588.1527; found 588.1535.

4',4'-Bis(4-methylaminophenyl)-3',3'-dimethyl-1-phenyl-1H-spiro[2,1-benzazaphosphole-1,2'-

[1,2]oxaphosphetan]-3(2H)-one (9i). Conversion 85%. Yield after precipitation from diethyl ether 73%. White solid. Mp 125-126 °C, decomp.

IR (KBr) ν 3444, 1665 cm^{-1} . ^1H NMR (300.13 MHz, CDCl_3): δ 8.72 (dddd,

$^3J_{PH} = 12.5$ Hz, $^3J_{HH} = 7.4$ Hz, $^4J_{HH} = 1.1$ Hz, $^5J_{HH} = 0.5$ Hz, 1H, H9), 7.98

(dddd, $^4J_{PH} = 3.1$ Hz, $^3J_{HH} = 7.4$ Hz, $^4J_{HH} = 1.1$ Hz, $^5J_{HH} = 0.5$ Hz, 1H, H12), 7.73-7.88 (m, 3H, H10,

H14), 7.67 (tdd, $^3J_{HH} = 7.4$ Hz, $^4J_{HH} = 1.1$ Hz, $^5J_{PH} = 2.0$ Hz, 1H, H11), 7.47 (dd, $^3J_{HH} = 8.7$, $^4J_{HH} =$

2.6 Hz, 2H, H20'), 7.21-7.33 (m, 5H, H15, H16, H20), 6.97 (d, $^2J_{PH} = 9.9$ Hz, 1H, H5), 6.63 (dd, $^3J_{HH}$

= 8.7, $^4J_{HH} = 2.5$ Hz, 2H, H21'), 6.46 (dd, $^3J_{HH} = 8.9$ Hz, $^4J_{HH} = 2.5$ Hz, 2H, H21), 2.84 (s, 6H, H23),

2.88 (s, 6H, H23'), 1.61 (d, $^3J_{PH} = 27.1$ Hz, 3H, H17), 1.26 (d, $^3J_{PH} = 27.0$ Hz, 3H, H18), ppm. $^{13}\text{C}\{^1\text{H}\}$

NMR (75.47 MHz, CDCl_3): δ 168.1 (d, $^2J_{PC} = 5.4$ Hz, C6), 148.7 (C22'), 148.6 (C22), 138.3 (d, $^2J_{PC}$

= 10.5 Hz, C7), 137.3 (d, $^1J_{PC} = 141.4$ Hz, C8), 136.5 (d, $^1J_{PC} = 151.3$ Hz, C13), 135.7 (d, $^2J_{PC} = 11.6$

Hz, C9), 135.0 (d, $^3J_{PC} = 10.5$ Hz, C19'), 133.4 (d, $^3J_{PC} = 4.7$ Hz, C19), 132.7 (d, $^4J_{PC} = 3.0$ Hz, C11),

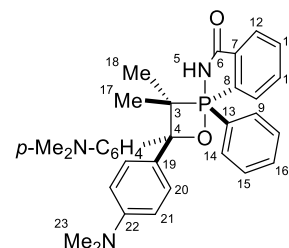
132.2 (d, $^2J_{PC} = 11.1$ Hz, C14), 131.9 (d, $^3J_{PC} = 15.1$ Hz, C10), 130.0 (d, $^4J_{PC} = 3.1$ Hz, C16), 127.9

(d, $^3J_{PC} = 14.6$ Hz, C15), 127.6 (C20), 126.8 (C20'), 124.4 (d, $^3J_{PC} = 12.0$ Hz, C12), 111.8 (C21'),

111.5 (C21), 79.7 (d, $^2J_{PC} = 13.7$ Hz, C4), 68.8 (d, $^1J_{PC} = 110.4$ Hz, C3), 40.5 (C23), 40.5 (C23'), 24.1

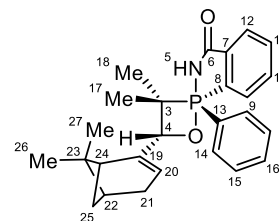
(d, $^2J_{PC} = 5.6$ Hz, C17), 23.9 (d, $^2J_{PC} = 5.4$ Hz, C18) ppm. $^{31}\text{P}\{^1\text{H}\}$ NMR (121.50 MHz, CDCl_3): δ -

64.2 ppm. HRMS (ESI/TOF) m/z: [M + 1] calcd for $\text{C}_{33}\text{H}_{37}\text{N}_3\text{O}_2\text{P}$, 538.2623; found 538.2625.



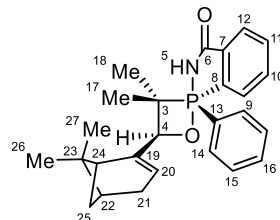
(1*S*,4'*R*)-4'-[(1*S*,5*R*)-6,6-dimethyl bicyclo[3.1.1]hept-2-en-2-yl]-3',3'-dimethyl-1-phenyl-1*H*-spiro[2,1-benzazaphosphole-1,2'-[1,2]oxaphosphetan]-3(2*H*)-one

(*trans*-**9k**).⁶⁹ Conversion 47%. Yield after chromatography (ethyl acetate:hexane 1:1) 39%. Slightly yellow oil. ¹H NMR (300.13 MHz, CDCl₃): δ 8.20 (m, 1H, H9), 7.97-8.08 (m, 3H, H14, H12), 7.61-7.72 (m, 2H, H10, H11), 7.38-7.53 (m, 3H, H15, H16), 6.00 (d, ²J_{PH} = 10.2 Hz, 1H, H-5), 5.64 (tq, ³J_{HH} = 3.0 Hz, ⁴J_{HH} = 1.5 Hz, 1H, H20), 4.25 (dq, ³J_{PH} = 5.5 Hz, ⁴J_{HH} = 1.5 Hz, 1H, H4), 2.37 (dt, ³J_{HH} = 5.6 Hz, ²J_{HH} = 8.4 Hz, 1H, H25), 2.33 (m, 2H, H21), 2.17 (t, ³J_{HH} = ⁴J_{HH} = 5.6 Hz, 1H, H24), 2.12 (m, 1H, H22), 1.39 (d, ³J_{PH} = 27.7 Hz, 3H, H17), 1.28 (s, 3H, H26), 1.20 (d, ²J_{PH} = 8.4 Hz, 1H, H25), 1.19 (d, ³J_{PH} = 26.0 Hz, 3H, H18), 0.93 (s, 3H, H27) ppm. ¹³C{¹H} NMR (75.47 MHz, CDCl₃): δ 168.6 (d, ²J_{PC} = 3.2 Hz, C6), 147.0 (d, ³J_{PC} = 16.7 Hz, C19), 137.8 (d, ²J_{PC} = 10.7 Hz, C7), 137.1 (d, ¹J_{PC} = 154.9 Hz, C8), 135.5 (d, ²J_{PC} = 12.1 Hz, C9), 134.8 (d, ²J_{PC} = 12.1 Hz, C14), 133.4 (d, ¹J_{PC} = 137.6 Hz, C13), 132.7 (d, ⁴J_{PC} = 3.0 Hz, C11), 131.9 (d, ³J_{PC} = 15.8 Hz, C10), 131.4 (d, ⁴J_{PC} = 3.8 Hz, C16), 128.6 (d, ³J_{PC} = 14.3 Hz, C15), 124.2 (d, ³J_{PC} = 12.8 Hz, C12), 119.8 (C20), 76.4 (d, ²J_{PC} = 17.4 Hz, C4), 66.4 (d, ¹J_{PC} = 107.8 Hz, C3), 43.0 (C24), 40.7 (C22), 37.8 (C23), 31.9 (C25), 31.3 (C21), 26.3 (C26), 23.8 (d, ²J_{PC} = 5.3 Hz, C17), 21.9 (C27), 19.4 (d, ²J_{PC} = 6.0 Hz, C18) ppm. ³¹P{¹H} NMR (121.50 MHz, CDCl₃): δ -63.7 ppm. HRMS (ESI/TOF) m/z: [M + 1] calcd for C₂₆H₃₁NO₂P, 420.2092; found 420.2099.



(1*R*,4'*R*)-4'-[(1*S*,5*R*)-6,6-dimethyl bicyclo[3.1.1]hept-2-en-2-yl]-3',3'-dimethyl-1-phenyl-1*H*-spiro[2,1-benzazaphosphole-1,2'-[1,2]oxaphosphetan]-3(2*H*)-one (*cis*-

9k). Conversion 49%. Yield after chromatography (ethyl acetate:hexane 1:1) 43%. Slightly yellow oil. ¹H NMR (300.13 MHz, CDCl₃): δ 8.25 (m, 1H, H9), 7.93-8.12 (m, 3H, H14, H12), 7.62-7.78 (m, 2H, H10, H11), 7.33-7.48 (m, 3H, H15, H16), 6.52 (d, ²J_{PH} = 10.7 Hz, 1H, H5), 5.65 (tq, ³J_{HH} = 3.0 Hz, ⁴J_{HH} = 1.5 Hz, 1H, H20), 4.18 (dq, ³J_{PH} = 7.0 Hz, ⁴J_{HH} = 1.5 Hz, 1H, H4), 2.32-2.48 (m, 3H, H25, H21), 2.12 (m, 1H, H22), 1.99 (t, ³J_{HH} = ⁴J_{HH} = 5.7, 1H, H24), 1.40 (d, ³J_{PH} = 26.4 Hz, 3H, H17), 1.16-1.31 (m, 7H, H18,

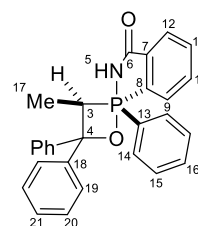


H25, H26), 0.95 (s, 3H, H27) ppm. $^{13}\text{C}\{^1\text{H}\}$ NMR (75.47 MHz, CDCl_3): δ 168.2 (d, $^2J_{\text{PC}} = 4.2$ Hz, C6), 146.9 (d, $^3J_{\text{PC}} = 13.2$ Hz, C19), 138.8 (d, $^2J_{\text{PC}} = 10.2$ Hz, C7), 135.4 (d, $^1J_{\text{PC}} = 147.2$ Hz, C13), 135.3 (d, $^2J_{\text{PC}} = 12.0$ Hz, C9), 134.9 (d, $^1J_{\text{PC}} = 143.6$ Hz, C8), 134.6 (d, $^2J_{\text{PC}} = 12.0$ Hz, C14), 133.1 (d, $^4J_{\text{PC}} = 3.0$ Hz, C11), 132.0 (d, $^3J_{\text{PC}} = 15.0$ Hz, C10), 131.1 (d, $^4J_{\text{PC}} = 3.6$ Hz, C16), 128.2 (d, $^3J_{\text{PC}} = 15.0$ Hz, C15), 124.7 (d, $^3J_{\text{PC}} = 11.4$ Hz, C12), 119.3 (C20), 77.6 (d, $^2J_{\text{PC}} = 17.4$ Hz, C4), 65.3 (d, $^1J_{\text{PC}} = 109.9$ Hz, C3), 43.1 (C24), 40.8 (C22), 37.7 (C23), 32.0 (C25), 31.3 (C21), 26.3 (C26), 24.3 (d, $^2J_{\text{PC}} = 5.8$ Hz, C17), 21.9 (C27), 19.6 (d, $^2J_{\text{PC}} = 5.8$ Hz, C18) ppm. $^{31}\text{P}\{^1\text{H}\}$ NMR (121.50 MHz, CDCl_3): δ -63.6 ppm. HRMS (ESI/TOF) m/z: [M + 1] calcd for $\text{C}_{26}\text{H}_{31}\text{NO}_2\text{P}$, 420.2092; found 420.2099.

(1*R, 3'*S*')-3'-methyl-1,4',4'-triphenyl-1*H*-spiro[2,1-benzazaphosphole-1,2'-[1,2]oxaphosphetan]-3(2*H*)-one** (*cis*-**9m**).⁶⁹ Conversion 86%. Yield after precipitation from

diethyl ether 80%. White solid. Mp 192-193 °C. IR (KBr) ν 3425, 3193, 1675 cm^{-1} .

^1H NMR (300.13 MHz, CDCl_3): δ 8.40 (m, 1H, H9), 7.85-8.01 (m, 3H, H12, H14), 7.79 (d, $^2J_{\text{PH}} = 11.0$ Hz, 1H, H5), 7.59-7.67 (m, 2H, H10, H11), 7.47-7.55



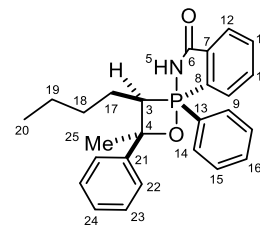
(m, 2H, H19'), 7.26-7.44 (m, 5H, H15, H16, H19), 7.08-7.25 (m, 6H, H20, H20', H21, H21'), 4.73 (dq, $^2J_{\text{PH}} = 24.1$ Hz, $^3J_{\text{HH}} = 8.1$ Hz, 1H, H3), 1.51 (dd, $^3J_{\text{PH}} = 29.2$ Hz, $^3J_{\text{HH}} = 8.1$ Hz, 3H, H17) ppm.

$^{13}\text{C}\{^1\text{H}\}$ NMR (75.47 MHz, CDCl_3): δ 167.4 (d, $^2J_{\text{PC}} = 7.2$ Hz, C6), 148.4 (d, $^3J_{\text{PC}} = 7.8$ Hz, C18'), 143.3 (d, $^3J_{\text{PC}} = 6.0$ Hz, C18), 138.2 (d, $^2J_{\text{PC}} = 12.0$ Hz, C7), 136.3 (d, $^1J_{\text{PC}} = 151.3$ Hz, C8), 136.1 (d, $^2J_{\text{PC}} = 12.6$ Hz, C9z), 136.0 (d, $^1J_{\text{PC}} = 143.0$ Hz, C13), 132.9 (d, $^4J_{\text{PC}} = 2.9$ Hz, C11), 132.5 (d, $^2J_{\text{PC}} = 11.4$ Hz, C14), 131.8 (d, $^3J_{\text{PC}} = 16.2$ Hz, C10), 130.5 (d, $^4J_{\text{PC}} = 3.6$ Hz, C16), 128.1 (d, $^3J_{\text{PC}} = 15.0$ Hz, C15), 128.0 (C20), 127.6 (C20'), 126.8 (C19), 126.6 (C21), 126.4 (C21'), 125.8 (C19'), 124.3 (d, $^3J_{\text{PC}} = 12.6$ Hz, C12), 77.5 (d, $^2J_{\text{PC}} = 15.0$ Hz, C4), 63.8 (d, $^1J_{\text{PC}} = 109.3$ Hz, C3), 13.4 (d, $^2J_{\text{PC}} = 9.6$ Hz, C17) ppm. $^{31}\text{P}\{^1\text{H}\}$ NMR (121.50 MHz, CDCl_3): δ -72.4 ppm. HRMS (ESI/TOF) m/z: [M + 1] calcd for $\text{C}_{26}\text{H}_{31}\text{NO}_2\text{P}$, 438.1623; found 438.1635.

(1*R*_P*,3'*S,4'*R**)-3'-buthyl-4'-methyl-1,4'-diphenyl-1*H*-spiro[2,1-benzazaphosphole-1,2'-[1,2]oxaphosphetan]-3(2*H*)-one** (*cis*-**9n**).⁶⁹ Conversion 87%. Yield after

precipitation from diethyl ether 78%. White solid. Mp 194-195 °C. IR (KBr)

ν 3425, 3235, 1678 cm⁻¹. ¹H NMR (300.13 MHz, CDCl₃): δ 8.50-8.60 (m,



1H, H9), 8.02-8.10 (m, 1H, H12), 7.79-7.91 (m, 2H, H14), 7.69-7.79 (m, 2H, H10, H11), 0.67 (t, ³J_{HH} = 6.7 Hz, 3H, H20), 7.28-7.46 (m, 4H, H5, H15, H16), 7.15-7.26 (m, 5H, H22, H23, H24), 3.81 (ddd,

²J_{PH} = 23.4 Hz, ³J_{HH} = 10.7 Hz, ³J_{HH} = 3.3 Hz, 1H, H3), 1.77 (s, 3H, H25), 1.47-1.68 (m, 2H, H17),

0.93-1.28 (m, 4H, H18, H19) ppm. ¹³C{¹H} NMR (75.47 MHz, CDCl₃): δ 167.3 (d, ²J_{PC} = 7.2 Hz,

C6), 143.6 (d, ³J_{PC} = 7.9 Hz, C21), 138.3 (d, ²J_{PC} = 11.5 Hz, C7), 137.3 (d, ¹J_{PC} = 149.6 Hz, C8),

136.1 (d, ²J_{PC} = 12.1 Hz, C9), 136.0 (d, ¹J_{PC} = 144.8 Hz, C13), 133.1 (d, ⁴J_{PC} = 3.0 Hz, C11), 132.3

(d, ²J_{PC} = 12.1 Hz, C14), 132.0 (d, ³J_{PC} = 15.6 Hz, C10), 130.5 (d, ⁴J_{PC} = 3.0 Hz, C16), 128.2 (d, ³J_{PC}

= 15.0 Hz, C15), 127.7 (C23), 126.8 (C24), 126.5 (C22), 124.5 (d, ³J_{PC} = 12.0 Hz, C12), 74.8 (d, ²J_{PC}

= 16.8 Hz, C4), 71.2 (d, ¹J_{PC} = 105.7 Hz, C3), 32.0 (d, ³J_{PC} = 6.0 Hz, C25), 31.1 (d, ³J_{PC} = 20.4 Hz,

C18), 26.6 (d, ²J_{PC} = 8.4 Hz, C17), 22.4 (d, ⁴J_{PC} = 1.8 Hz, C19), 13.6 (C20) ppm. ³¹P{¹H} NMR

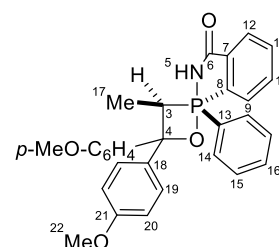
(121.50 MHz, CDCl₃): δ -75.9 ppm. HRMS (ESI/TOF) m/z: [M + 1] calcd for C₂₆H₂₉NO₂P,

418.1936; found 418.1952.

(1*R*_P*, 3'*S)-4',4'-Bis(4-methoxyphenyl)-3'-methyl-1-phenyl-1*H*-spiro[2,1-benzazaphosphole-1,2'-[1,2]oxaphos-phetan]-3(2*H*)-one** (*cis*-**9o**). Conversion 83%. Yield

after precipitation from diethyl ether 75%. White solid. Mp 138-140 °C,

decomp. IR (KBr) ν 1683 cm⁻¹. ¹H NMR (300.13 MHz, CDCl₃): δ 8.39



(m, 1H, H9), 7.96 (m, 1H, H12), 7.84 (m, 2H, H14), 7.59-7.66 (m, 2H,

H10, H11), 7.32-7.44 (m, 5H, H15, H16, H19'), 7.08 (dd, ³J_{HH} = 8.8, ⁴J_{HH} = 2.5 Hz, 2H, H19), 6.95

(d, ²J_{PH} = 11.3 Hz, 1H, H5), 6.81 (dd, ³J_{HH} = 8.6, ⁴J_{HH} = 2.5 Hz, 2H, H20'), 6.67 (dd, ³J_{HH} = 8.8 Hz,

⁴J_{HH} = 2.5 Hz, 2H, H20), 4.69 (dq, ²J_{PH} = 24.0 Hz, ³J_{HH} = 7.9 Hz, 1H, H3), 3.76 (s, 3H, H22'), 3.73

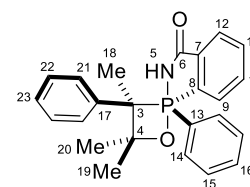
(s, 3H, H22), 1.47 (dd, ³J_{PH} = 29.2 Hz, ³J_{HH} = 7.9 Hz, 3H, H17) ppm. ¹³C{¹H} NMR (75.47 MHz,

CDCl₃): δ 167.9 (d, ²J_{PC} = 7.5 Hz, C6), 158.2 (C21'), 157.9 (C21), 139.9 (d, ³J_{PC} = 8.3 Hz, C18'),

1
2 138.1 (d, $^2J_{PC} = 10.9$ Hz, C7), 136.3 (d, $^3J_{PC} = 5.2$ Hz, C18), 136.1 (d, $^1J_{PC} = 149.8$ Hz, C8), 136.1 (d,
3
4 $^2J_{PC} = 12.1$ Hz, C9), 135.9 (d, $^1J_{PC} = 141.0$ Hz, C13), 133.0 (d, $^4J_{PC} = 3.1$ Hz, C11), 132.3 (d, $^2J_{PC} =$
5
6 11.4 Hz, C14), 131.9 (d, $^3J_{PC} = 15.3$ Hz, C10), 130.5 (d, $^4J_{PC} = 3.3$ Hz, C16), 128.2 (d, $^3J_{PC} = 14.9$ Hz,
7
8 C15), 127.9 (C19), 126.9 (C19'), 124.3 (d, $^3J_{PC} = 12.4$ Hz, C12), 113.3 (C20'), 112.9 (C20), 79.4 (d,
9
10 $^2J_{PC} = 13.7$ Hz, C4), 63.7 (d, $^1J_{PC} = 109.0$ Hz, C3), 55.1 (C22'), 55.1 (C-22), 13.5 (d, $^2J_{PC} = 9.3$ Hz,
11
12 C17) ppm. $^{31}\text{P}\{^1\text{H}\}$ NMR (121.50 MHz, CDCl_3): δ -72.8 ppm. HRMS (ESI/TOF) m/z: [M + 1] calcd
13
14 for $\text{C}_{30}\text{H}_{29}\text{NO}_4\text{P}$, 418.1834; found 418.1849.

15
16
17
18
19 **(1*R*_P*,3'*R**)-3',4',4'-trimethyl-1,3'-diphenyl-1,2-dihydro-3*H*-1 λ^5 -spiro[benzo[*c*][1,2]aza-**
20
21 **phosphole-1,2'-[1,2]oxaphosphetan]-3-one (*cis*-9*p*).** Conversion 18%.

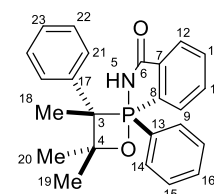
22
23 Yield after two successive chromatographic purifications (ethyl
24
25 acetate:hexane 2:3) 1%. White solid. Mp 168-170 °C, decomp. IR (KBr) ν



26
27 1668 cm^{-1} . ^1H NMR (300.13 MHz, CDCl_3): δ 8.33 (m, 2H, H14), 8.13 (m, 1H, H9), 8.02 (m, 1H,
28
29 H12), 7.65 (m, 1H, H10), 7.62 (m, 1H, H11), 7.5 (m, 1H, H16), 7.47 (m, 2H, H15), 7.25 (m, 5H, H21,
30
31 H22, H23), 6.19 (d, $^2J_{PH} = 11.8$ Hz, H5), 1.76 (d, $^3J_{PH} = 27.1$ Hz, 3H, H18), 1.47 (s, 3H, H20), 1.10
32
33 (s, 3H, H19) ppm. $^{13}\text{C}\{^1\text{H}\}$ NMR (75.47 MHz, CDCl_3): δ 168.8 (d, $^2J_{PC} = 4.7$ Hz, C6), 141.1 (d, $^2J_{PC}$
34
35 = 7.7 Hz, C17), 139.2 (d, $^1J_{PC} = 152.3$ Hz, C8), 137.8 (d, $^2J_{PC} = 10.5$ Hz, C7), 134.6 (d, $^2J_{PC} = 11.7$
36
37 Hz, C9), 136.6 (d, $^2J_{PC} = 13.0$ Hz, C14), 136.4 (d, $^1J_{PC} = 134.4$ Hz, C13), 132.8 (d, $^4J_{PC} = 3.0$ Hz,
38
39 C11), 132.3 (d, $^3J_{PC} = 15.6$ Hz, C10), 132.0 (d, $^4J_{PC} = 3.6$ Hz, C16), 129.1 (d, $^3J_{PC} = 14.6$ Hz, C15),
40
41 127.6 (d, $^3J_{PC} = 15.1$ Hz, C21), 128.9 (C22), 124.7 (d, $^3J_{PC} = 12.3$ Hz, C12), 127.4 (C23), 75.2 (d,
42
43 $^1J_{PC} = 115.4$ Hz, C3), 73.4 (d, $^2J_{PC} = 16.1$ Hz, C4), 29.7 (d, $^3J_{PC} = 2.7$ Hz, C19), 26.7 (d, $^3J_{PC} = 11.5$
44
45 Hz, C20), 21.2 (d, $^2J_{PC} = 6.9$ Hz, C18) ppm. $^{31}\text{P}\{^1\text{H}\}$ NMR (121.50 MHz, CDCl_3): δ -67.5 ppm.
46
47
48
49
50
51
52
53 HRMS (ESI/TOF) m/z: [M + 1] calcd for $\text{C}_{24}\text{H}_{25}\text{NO}_2\text{P}$, 390.1623; found 390.1639.

54
55 **(1*R*_P*,3'*S**)-3',4',4'-trimethyl-1,3'-diphenyl-1,2-dihydro-3*H*-1 λ^5 -spiro[benzo[*c*][1,2]aza-**
56
57 **phosphole-1,2'-[1,2]oxaphosphetan]-3-one (*trans*-9*p*).** Identified from a

58
59 mixture of *cis*-9*p*:*trans*-9*p* in a ratio of 76:24 obtained after purification of a crude
60
61 reaction mixture through two successive column chromatography separations

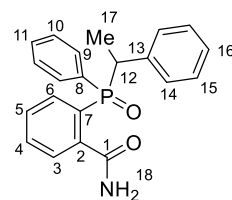


using ethyl acetate:hexane 2:3 as eluent. Conversion 9%. Yield 0.3%. The amount obtained was too small to achieve the characterization of the mixture. Only the ^1H and ^{31}P NMR data are provided. ^1H NMR (300.13 MHz, CDCl_3): δ 8.08-8.28 (m, 3H, H9, H14), 8.02 (m, 1H, H12), 7.35-7.75 (m, 5H, H11, H10, H15, H16), 7.11-7.21 (m, 5H, H21, H22, H23), 6.07 (d, $^2J_{\text{PH}} = 11.7$ Hz, H5), 1.85 (d, $^3J_{\text{PH}} = 28.4$ Hz, 3H, H18), 1.34 (s, 3H, H20*), 0.95 (s, 3H, H19*) ppm. *Interchangables. $^{31}\text{P}\{^1\text{H}\}$ NMR (121.50 MHz, CDCl_3): δ -68.73 ppm.

2-(phenyl(1-phenylethyl)phosphoryl)benzamide (13). Conversion 35%. Yield

after chromatography (ethyl acetate:hexane 2:3) 18%. White solid. Mp. 277-278

$^\circ\text{C}$. IR (KBr): ν 3452, 3130, 1667, 1619, 1166 cm^{-1} . ^1H NMR (300.13 MHz,



CD_3OD): δ 7.80 (m, 3H, H6, H9), 7.53 (m, 3H, H10, H11), 7.42 (m, 2H, H4,

H3), 7.35 (m, 3H, H5, H14), 7.08 (m, 3H, H15, H16), 4.76 (m, 1H, H12), 1.75 (dd, $^3J_{\text{PH}} = 16.8$ Hz,

$^3J_{\text{HH}} = 7.4$ Hz, 3H, H17) ppm. $^{13}\text{C}\{^1\text{H}\}$ NMR (75.47 MHz, CD_3OD): δ 171.7 (d, $^3J_{\text{PC}} = 3.6$ Hz, C1),

138.5 (d, $^2J_{\text{PC}} = 8.8$ Hz, C2), 138.1 (d, $^2J_{\text{PC}} = 6.5$ Hz, C13), 133.5 (d, $^2J_{\text{PC}} = 5.8$ Hz, C6), 131.8 (d,

$^2J_{\text{PC}} = 9.2$ Hz, C9), 131.4 (d, $^1J_{\text{PC}} = 96.3$ Hz, C8), 131.4 (d, $^4J_{\text{PC}} = 2.8$ Hz, C11), 131.1 (d, $^4J_{\text{PC}} = 2.6$

Hz, C4), 130.6 (d, $^1J_{\text{PC}} = 96.0$ Hz, C7), 129.0 (d, $^3J_{\text{PC}} = 10.4$ Hz, C5), 128.7 (d, $^3J_{\text{PC}} = 5.7$ Hz, C14),

127.9 (d, $^3J_{\text{PC}} = 11.6$ Hz, C10), 127.5 (d, $^4J_{\text{PC}} = 2.5$ Hz, C15), 127.2 (d, $^3J_{\text{PC}} = 9.7$ Hz, C3), 126.4 (d,

$^5J_{\text{PC}} = 3.1$ Hz, C16), 38.0 (d, $^1J_{\text{PC}} = 68.4$ Hz, C12), 14.4 (d, $^2J_{\text{PC}} = 3.8$ Hz, C17) ppm. $^{31}\text{P}\{^1\text{H}\}$ NMR

(121.50 MHz, CD_3OD): δ 41.48 ppm. HRMS (ESI/TOF) m/z : $[\text{M} + 1]$ calcd for $\text{C}_{21}\text{H}_{21}\text{NO}_2\text{P}$,

350.1310; found 350.1316.

General procedure for the synthesis of spiro-1,2-oxaphosphetanes 12a-d. To a solution of the

appropriate phosphazene **7** (6.64×10^{-4} mol) in THF (10 mL) was added a solution of *t*-BuLi (0.86

mL of a 1.7 M solution in cyclohexane, 1.46×10^{-3} mol) at -35 $^\circ\text{C}$. After 30 min of metallation was

added the corresponding electrophile (0.66×10^{-3} mol) at -90 $^\circ\text{C}$ and the mixture was stirred during 2

h and 30 min. Then, the reaction was quenched with methyl trifluoromethanesulfonate (MeOTf, 0.09

mL, 7.97×10^{-4} mol) and stirred during 30 min at -35 $^\circ\text{C}$. The reaction mixture was poured into water

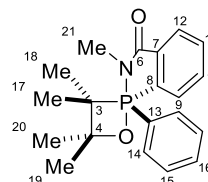
and extracted with dichloromethane (2x15 mL). The organic layers were dried over Na_2SO_4 and

concentrated in vacuo affording a white solid. ^1H , $^1\text{H}\{^{31}\text{P}\}$, and $^{31}\text{P}\{^1\text{H}\}$ NMR spectra of the crude reaction were always measured in order to determine the conversion of the process. The crude mixture was purified by precipitation from diethyl ether affording **12a-d**.

2,3',3',4',4'-Pentamethyl-1-phenyl-1*H*-spiro[2,1-benzazaphosphole-1,2'-[1,2]oxaphosphetan]-3(2*H*)-one (12a). Conversion 95%. Yield after precipitation from diethyl ether

88%. White solid. Mp 163-164 °C. IR (KBr) ν 1635 cm^{-1} . ^1H NMR (300.13 MHz,

CDCl_3): δ 8.03-8.14 (m, 2H, H9, H12), 7.62-7.73 (m, 3H, H11, H14), 7.58 (ddt,



$^3J_{\text{HH}} = 7.5$ Hz, $^4J_{\text{PH}} = 4.9$ Hz, $^4J_{\text{HH}} = 1.4$ Hz, 1H, H10), 7.28-7.45 (m, 2H, H15, H16), 2.62 (d, $^3J_{\text{PH}} =$

3.0 Hz, 3H, H21), 1.68 (d, $^3J_{\text{PH}} = 25.2$ Hz, 3H, H17), 1.18 (s, 3H, H20), 1.51 (s, 3H, H19), 1.00 (d,

$^3J_{\text{PH}} = 27.7$ Hz, 3H, H18) ppm. $^{13}\text{C}\{^1\text{H}\}$ NMR (75.47 MHz, CDCl_3): δ 166.8 (d, $^2J_{\text{PC}} = 6.5$ Hz, C6),

139.5 (d, $^2J_{\text{PC}} = 10.2$ Hz, C7), 135.8 (d, $^2J_{\text{PC}} = 11.7$ Hz, C9), 134.6 (d, $^2J_{\text{PC}} = 12.2$ Hz, C14), 134.2 (d,

$^1J_{\text{PC}} = 139.4$ Hz, C13), 133.0 (d, $^4J_{\text{PC}} = 3.2$ Hz, C11), 132.9 (d, $^1J_{\text{PC}} = 144.4$ Hz, C8), 131.3 (d, $^4J_{\text{PC}} =$

2.9 Hz, C16), 131.2 (d, $^3J_{\text{PC}} = 15.6$ Hz, C10), 128.6 (d, $^3J_{\text{PC}} = 15.0$ Hz, C15), 124.2 (d, $^3J_{\text{PC}} = 11.4$

Hz, C12), 73.7 (d, $^2J_{\text{PC}} = 16.1$ Hz, C4), 66.0 (d, $^1J_{\text{PC}} = 106.9$ Hz, C3), 29.7 (C21), 27.1 (d, $^3J_{\text{PC}} = 1.7$

Hz, C19), 25.7 (d, $^3J_{\text{PC}} = 11.0$ Hz, C20), 21.7 (d, $^2J_{\text{PC}} = 6.6$ Hz, C18), 20.5 (d, $^2J_{\text{PC}} = 5.2$ Hz, C17)

ppm. $^{31}\text{P}\{^1\text{H}\}$ NMR (121.50 MHz, CDCl_3): δ -53.4 ppm. HRMS (ESI/TOF) m/z : $[M + 1]$ calcd for

$\text{C}_{20}\text{H}_{25}\text{NO}_2\text{P}$, 342.1623; found 342.1641.

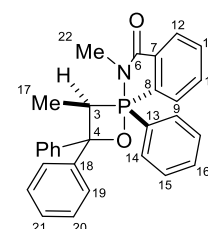
(2'*R*_P*,3'*S)-2,3'-dimethyl-1,4',4'-triphenyl-1*H*-spiro[2,1-benzazaphosphole-1,2'-**

[1,2]oxaphosphetan]-3(2*H*)-one (*cis*-12b). Conversion 87%. Yield after

precipitation from diethyl ether 80%. White solid. Mp 163-165 °C. IR (KBr) ν

1665 cm^{-1} . ^1H NMR (300.13 MHz, CDCl_3): δ 8.02 (dd, $^4J_{\text{PH}} = 3.1$ Hz, $^3J_{\text{HH}} = 7.5$

Hz, 1H, H12), 7.90 (dd, $^3J_{\text{PH}} = 13.3$ Hz, $^3J_{\text{HH}} = 7.5$ Hz, 1H, H9), 7.64 (m, 2H,



H14), 7.50-7.58 (m, 3H, H11, H19), 7.37-7.49 (m, 5H, H15, H16, H20), 7.23-7.36 (m, 4H, H19',

H21, H10), 7.12-7.19 (m, 2H, H20'), 7.01-7.10 (m, 1H, H21'), 4.70 (dq, $^2J_{\text{PH}} = 19.7$ Hz, $^3J_{\text{HH}} = 8.0$

Hz, 1H, H3), 2.64 (d, $^3J_{\text{PH}} = 2.6$ Hz, 3H, H22), 1.64 (d, $^3J_{\text{HH}} = 8.0$ Hz, $^3J_{\text{PH}} = 28.2$ Hz, 3H, H17) ppm.

$^{13}\text{C}\{^1\text{H}\}$ NMR (75.47 MHz, CDCl_3): δ 166.1 (d, $^2J_{\text{PC}} = 8.4$ Hz, C6), 147.2 (d, $^3J_{\text{PC}} = 4.2$ Hz, C18'),

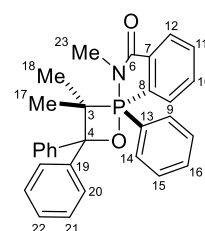
1
2 143.9 (d, $^3J_{PC} = 10.2$ Hz, C18), 138.9 (d, $^2J_{PC} = 12.0$ Hz, C7), 136.4 (d, $^2J_{PC} = 12.0$ Hz, C9), 133.3 (d,
3
4 $^1J_{PC} = 146.6$ Hz, C13), 132.8 (d, $^4J_{PC} = 3.0$ Hz, C11), 132.7 (d, $^1J_{PC} = 144.8$ Hz, C8), 132.3 (d, $^2J_{PC} =$
5
6 12.6 Hz, C14), 130.9 (d, $^4J_{PC} = 3.6$ Hz, C16), 130.7 (d, $^3J_{PC} = 15.0$ Hz, C10), 128.6 (d, $^3J_{PC} = 15.7$
7
8 Hz, C15), 128.1 (C20), 127.8 (C20'), 126.6 (C19), 126.6 (C21), 126.5 (C21'), 126.2 (C19'), 123.9 (d,
9
10 $^3J_{PC} = 12.0$ Hz, C12), 78.2 (d, $^2J_{PC} = 15.0$ Hz, C4), 63.7 (d, $^1J_{PC} = 108.7$ Hz, C3), 29.7 (C22), 14.0 (d,
11
12 $^2J_{PC} = 10.0$ Hz, C17) ppm. $^{31}\text{P}\{^1\text{H}\}$ NMR (121.50 MHz, CDCl_3): δ -59.8 ppm. HRMS (ESI/TOF)
13
14 m/z: $[\text{M} + 1]$ calcd for $\text{C}_{29}\text{H}_{27}\text{NO}_2\text{P}$, 452.1779; found 452.1793.

15
16
17
18 **2,3',3'-Trimethyl-1,4',4'-triphenyl-1*H*-spiro[2,1-benzazaphosphole-1,2'-[1,2]oxa-phosphetan]-**
19

20
21 **3(2*H*)-one (12c)**. Conversion 95%. Yield after precipitation from diethyl ether

22 90%. White solid. Mp 179-180 °C. IR (KBr) ν 1653 cm^{-1} . ^1H NMR (300.13 MHz,

23 CDCl_3): δ 8.42 (dd, $^3J_{\text{PH}} = 12.6$ Hz, $^3J_{\text{HH}} = 7.5$ Hz, 1H, H9), 8.07 (ddd, $^4J_{\text{PH}} = 3.5$

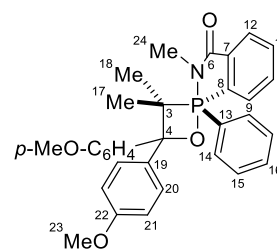


24 Hz, $^3J_{\text{HH}} = 7.3$ Hz, $^4J_{\text{HH}} = 0.9$ Hz, 1H, H12), 7.66-7.71 (m, 2H, H20'), 7.60-7.65 (m, 3H, H10, H14),
25
26 7.54-7.59 (m, 1H, H11), 7.29-7.53 (m, 6H, H15, H16, H20, H21'), 7.15-7.27 (m, 3H, H2, H22'),
27
28 7.01-7.10 (m, 1H, H22), 2.54 (d, $^3J_{\text{PH}} = 28.3$ Hz, 3H, H23), 1.79 (d, $^3J_{\text{PH}} = 25.2$ Hz, 3H, H17), 1.36
29
30 (d, $^3J_{\text{PH}} = 28.3$ Hz, 3H, H18) ppm. $^{13}\text{C}\{^1\text{H}\}$ NMR (75.47 MHz, CDCl_3): δ 166.8 (d, $^2J_{PC} = 7.2$ Hz,
31
32 C6), 145.1 (d, $^3J_{PC} = 7.6$ Hz, C19'), 145.1 (d, $^3J_{PC} = 7.2$ Hz, C19), 139.0 (d, $^2J_{PC} = 11.3$ Hz, C7), 136.0
33
34 (d, $^2J_{PC} = 12.1$ Hz, C9), 134.0 (d, $^1J_{PC} = 137.3$ Hz, C8), 133.1 (d, $^1J_{PC} = 155.4$ Hz, C13), 133.0 (d,
35
36 $^4J_{PC} = 3.0$ Hz, C11), 131.9 (d, $^2J_{PC} = 12.2$ Hz, C14), 131.1 (d, $^3J_{PC} = 15.0$ Hz, C10), 130.5 (d, $^4J_{PC} =$
37
38 3.4 Hz, C16), 128.3 (d, $^3J_{PC} = 15.5$ Hz, C15), 127.9 (C21), 127.5 (C21'), 126.5 (C20 and C20'), 126.3
39
40 (C22), 126.2 (C22'), 124.0 (d, $^3J_{PC} = 11.6$ Hz, C12), 80.4 (d, $^2J_{PC} = 13.5$ Hz, C4), 68.1 (d, $^1J_{PC} = 110.8$
41
42 Hz, C3), 24.7 (d, $^2J_{PC} = 7.0$ Hz, C18), 30.5 (C23), 24 (d, $^2J_{PC} = 4.7$ Hz, C17) ppm. $^{31}\text{P}\{^1\text{H}\}$ NMR
43
44 (121.50 MHz, CDCl_3): δ -48.9 ppm. HRMS (ESI/TOF) m/z: $[\text{M} + 1]$ calcd for $\text{C}_{30}\text{H}_{29}\text{NO}_2\text{P}$,
45
46 466.1936; found 466.1952.
47
48
49
50
51
52
53
54
55
56
57
58
59
60

4',4'-bis(4-methoxyphenyl)-2,3',3'-trimethyl-1-phenyl-1H-spiro[2,1-benzazaphosphole-1,2'-[1,2]oxaphosphetan]-3(2H)-one (12d). Conversion 91%. Yield after

precipitation from diethyl ether 87%. White solid. Mp 183-184 °C. IR (KBr)

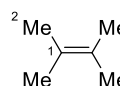
ν 1685 cm^{-1} . ^1H NMR (300.13 MHz, CDCl_3): δ 8.39 (dddd, $^3J_{\text{PH}} = 13.0$ Hz, $^3J_{\text{HH}} = 7.5$ Hz, $^4J_{\text{HH}} = 1.2$ Hz, $^5J_{\text{HH}} = 0.5$ Hz, 1H, H9), 8.06 (dddd, $^4J_{\text{PH}} = 3.5$



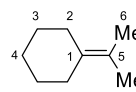
Hz, $^3J_{\text{HH}} = 7.5$ Hz, $^4J_{\text{HH}} = 1.2$ Hz, $^5J_{\text{HH}} = 0.5$ Hz, 1H, H12), 7.66 (tdd, $^3J_{\text{HH}} = 7.4$ Hz, $^4J_{\text{HH}} = 1.2$ Hz, $^5J_{\text{PH}} = 2.0$ Hz, 1H, H11), 7.38-7.62 (m, 8H, H16, H20, H20', H14, H10), 6.89 (dd, $^3J_{\text{HH}} = 8.9$ Hz, $^4J_{\text{HH}} = 2.5$ Hz, 2H, H21), 7.33 (m, 2H, H15), 6.72 (dd, $^3J_{\text{HH}} = 8.9$ Hz, $^4J_{\text{HH}} = 2.5$ Hz, 2H, H21'), 3.83 (s, 3H, H23), 3.71 (s, 3H, H23'), 2.53 (d, $^3J_{\text{PH}} = 2.9$ Hz, 3H, H24), 1.76 (d, $^3J_{\text{PH}} = 25.4$ Hz, 3H, H17), 1.32 (d, $^3J_{\text{PH}} = 28.3$ Hz, 3H, H18) ppm. ^{13}C $\{^1\text{H}\}$ NMR (75.47 MHz, CDCl_3): δ 167 (d, $^2J_{\text{PC}} = 6.4$ Hz, C6), 157.9 (C22'), 157.7 (C22), 139.5 (d, $^2J_{\text{PC}} = 10.2$ Hz, C7), 138.8 (d, $^3J_{\text{PC}} = 6.1$ Hz, C19'), 138.6 (d, $^3J_{\text{PC}} = 8.8$ Hz, C19), 135.9 (d, $^2J_{\text{PC}} = 12.1$ Hz, C9), 134.7 (d, $^1J_{\text{PC}} = 146.1$ Hz, C13), 133 (d, $^4J_{\text{PC}} = 2.9$ Hz, C11), 132.5 (d, $^1J_{\text{PC}} = 143.2$ Hz, C8), 131.8 (d, $^2J_{\text{PC}} = 12.3$ Hz, C14), 131.1 (d, $^3J_{\text{PC}} = 15.1$ Hz, C10), 130.4 (d, $^4J_{\text{PC}} = 3.5$ Hz, C16), 128.3 (d, $^3J_{\text{PC}} = 15.3$ Hz, C15), 127.5 (C20), 127.4 (C20'), 124 (d, $^3J_{\text{PC}} = 11.6$ Hz, C12), 113.2 (C21'), 112.8 (C21), 80.7 (d, $^2J_{\text{PC}} = 12.9$ Hz, C4), 70.4 (d, $^1J_{\text{PC}} = 107.9$ Hz, C3), 55.2 (C23'), 55 (C23), 30.4 (C24), 24.7 (d, $^2J_{\text{PC}} = 6.9$ Hz, C18), 24 (d, $^2J_{\text{PC}} = 4.6$ Hz, C17) ppm. ^{31}P $\{^1\text{H}\}$ NMR (121.50 MHz, CDCl_3): δ -48.7 ppm. HRMS (ESI/TOF) m/z: $[\text{M} + 1]$ calcd for $\text{C}_{32}\text{H}_{33}\text{NO}_4\text{P}$, 526.2147; found 526.2156.

General procedure for the synthesis of olefins 10 and benzoazaphospholes 11 and 14. A solution of the appropriate 1,2-oxaphosphetane **9/12c** (1.3×10^{-4} mol) in $\text{DMSO}-d_6$ (0.5 mL) was heated at 140 °C. After 14 hours, 15 mL of water were added and the reaction mixture was extracted with CH_2Cl_2 (2x20 mL). Then the organic layers were dried over Na_2SO_4 and concentrated *in vacuo*. The olefin **10** was extracted with hexane (2x5 mL) and the insoluble residue was washed with diethyl ether and identified as the benzoazaphosphol **11/14**. All olefins obtained have been described in the literature.

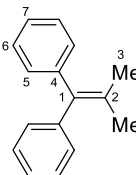
2,3-Dimethyl-2-butene (10a). Conversion >97%. Identified from the crude reaction mixture. ¹H NMR (300.13 MHz, DMSO-*d*₆): δ 1.85 (s, 12H, H₂) ppm. ¹³C NMR (75.47 MHz, CDCl₃): δ 124.5 (C₁), 20.4 (C₂) ppm.



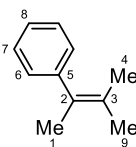
(1-methylethylidene)cyclohexane (10b). Conversion >97%. Colorless oil. Yield: 90%. ¹H NMR (300.13 MHz, CDCl₃): δ 2.06 (m, 4H, H₂), 1.55 (m, 6H, H₆), 1.47 (m, 6H, H₃ and H₄) ppm.



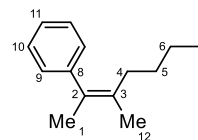
1,1'-(2-methylprop-1-ene-1,1-diyl)dibenzene (10c). Conversion >97%. Colorless oil. Yield: 94%. ¹H NMR (300.13 MHz, CDCl₃): δ 7.30 (m, 2H, H₅), 7.21 (m, 1H, H₇), 7.16 (m, 2H, H₆), 1.83 (s, 3H, H₃) ppm. ¹³C NMR (75.47 MHz, CDCl₃): δ 143.3 (C₄), 137.1 (C₁), 131.0 (C₂), 129.8 (C₅), 127.8 (C₆), 126.0 (C₇), 24.4 (C₃) ppm.



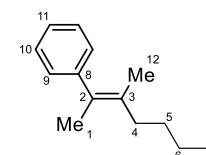
(1,2-Dimethyl-1-propen-1-yl)-benzene (10d). Conversion >97%. Colorless oil. Yield: 92%. ¹H NMR (300.13 MHz, CDCl₃): δ 7.29 (m, 2H, H₇), 7.17 (m, 1H, H₈), 7.09 (m, 2H, H₆), 1.90 (s, 3H, H₉), 1.76 (s, 3H, H₄), 1.53 (s, 3H, H₁) ppm.



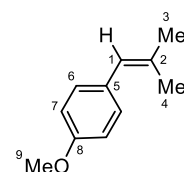
(Z)-(3-methylhept-2-en-2-yl)benzene (Z-10e). Conversion >97%. Colorless oil. Yield: 95%. ¹H NMR (300.13 MHz, CDCl₃): δ 7.30 (m, 2H, H₁₀), 7.19 (m, 1H, H₁₁), 7.07 (d, ³J_{HH} = 7.5 Hz, 2H, H₉), 2.00 (t, ³J_{HH} = 7.5 Hz, 2H, H₄), 1.95 (s, 3H, H₁₂), 1.74 (s, 3H, H₁), 1.10-1.35 (m, 4H, H₅, H₆), 0.80 (t, ³J_{HH} = 7.4 Hz, 3H, H₇) ppm.



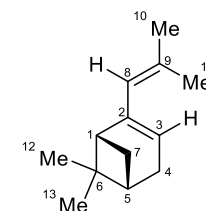
(E)-(3-methylhept-2-en-2-yl)benzene (E-10e). Conversion >97%. Colorless oil. Yield: 96%. ¹H NMR (300.13 MHz, CDCl₃): δ 7.32 (m, 2H, H₁₀), 7.19 (m, 1H, H₁₁), 7.12 (d, ³J_{HH} = 7.7 Hz, 2H, H₉), 2.19 (t, ³J_{HH} = 7.5 Hz, 2H, H₄), 1.58 (s, 3H, H₁), 1.98 (s, 3H, H₁₂), 1.45 (m, 4H, H₅, H₆), 0.98 (t, ³J_{HH} = 7.2 Hz, 3H, H₇) ppm.



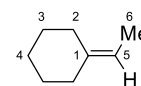
1-Methoxy-4-(2-dimethyl-1-propen-1-yl)-benzene (10j). Conversion >97%. Colorless oil. Yield: 95%. ¹H NMR (300.13 MHz, CDCl₃): δ 7.19 (d, ³J_{HH} = 8.9 Hz, 2H, H₆), 6.88 (d, ³J_{HH} = 8.9 Hz, 2H, H₇), 6.25 (s, 1H, H₁), 3.83 (s, 3H, H₉), 1.92 (s, 3H, H₃), 1.88 (s, 3H, H₄) ppm.



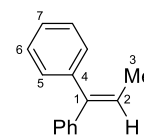
(1R,5S)-6,6-dimethyl-2-(2-methylprop-1-enyl)bicyclo[3.1.1]hept-2-ene (dimethylnopadiene, 10k). Conversion >97%. Colorless oil. Yield: 95%. ¹H NMR (300.13 MHz, CDCl₃): δ 5.56 (m, 1H, H₈), 5.38 (m, 1H, H₃), 2.39 (dt, ⁴J_{HH} = 5.6 Hz, ²J_{HH} = 8.5 Hz, 1H, H₇), 2.35 (m, 2H, H₄), 2.21 (td, ³J_{HH} = ⁴J_{HH} = 5.6 Hz, ⁴J_{HH} = 1.6 Hz, 1H, H₁), 2.10 (m, 1H, H₅), 1.79 (bs, 3H, H₁₀ or H₁₁), 1.78 (bs, 3H, H₁₀ or H₁₁), 1.30 (s, 3H, H₁₂ or H₁₃), 1.22 (d, 1H, ³J_{HH} = 8.5 Hz, H₇), 0.90 (s, 3H, H₁₂ or H₁₃) ppm. ¹³C NMR (75.47 MHz, CDCl₃): δ 145.5 (C, C₂), 132.7 (C, C₉), 126.1 (CH, C₈), 120.4 (CH, C₃), 46.7 (CH, C₁), 40.5 (CH, C₅), 37.7 (C, C₆), 31.7 (CH₂, C₄), 31.5 (CH₂, C₇), 26.7 (CH₃, C₁₀ or C₁₁), 26.3 (CH₃, C₁₂ or C₁₃), 21.1 (CH₃, C₁₂ or C₁₃), 19.9 (CH₃, C₁₀ or C₁₁) ppm.



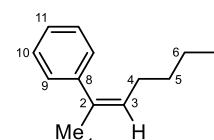
Ethylidenecyclohexane (10l). Conversion >97%. Colorless oil. Yield: 92%. ¹H NMR (300.13 MHz, CDCl₃): δ 5.06 (q, ³J_{HH} = 6.7 Hz, 1H, H5), 2.06 (m, 2H, H2), 2.00 (m, 2H, H2), 1.51 (d, ³J_{HH} = 6.7 Hz, 3H, H6), 1.47 (m, 6H, H3, H4) ppm.



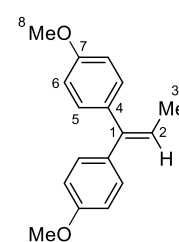
1,1'-Prop-1-ene-1,1-diyl dibenzene (10m). Conversion >97%. Colorless oil. Yield: 94%. ¹H NMR (300.13 MHz, CDCl₃): δ 7.22-7.38 (m, 4H, H6), 7.05-7.21 (m, 6H, H5, H7), 6.21 (q, ³J_{HH} = 7.0 Hz, 1H, H2), 1.69 (d, ³J_{HH} = 7.0 Hz, 3H, H3) ppm.



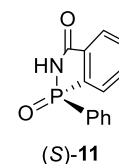
(Z)-hept-2-en-2-ylbenzene (10n). Conversion >97%. Colorless oil. Yield: 94%. ¹H NMR (300.13 MHz, CDCl₃): δ 7.28 (m, 2H, H10), 7.21 (m, 1H, H11), 7.12 (m, 2H, H9), 5.47 (t, ³J_{HH} = 6.9 Hz, 3H, H3), 2.51 (m, 2H, H4), 2.03 (s, 3H, H1), 1.07-1.37 (m, 4H, H5, H6), 0.83 (t, ³J_{HH} = 7.2 Hz, 3H, H7) ppm.



1,1'-prop-1-ene-1,1-diylbis(4-methoxybenzene) (10o). Conversion >97%. Colorless oil. Yield: 94%. ¹H NMR (300.13 MHz, CDCl₃): δ 6.81 (dd, ³J_{HH} = 8.8 Hz, ⁴J_{HH} = 2.6 Hz, 2H, H5'), 7.12 (dd, ³J_{HH} = 8.8 Hz, ⁴J_{HH} = 2.6 Hz, 2H, H5), 6.92 (dd, ³J_{HH} = 8.8 Hz, ⁴J_{HH} = 2.6 Hz, 2H, H6'), 6.81 (dd, ³J_{HH} = 8.8 Hz, ⁴J_{HH} = 2.6 Hz, 2H, H6), 6.04 (q, ³J_{HH} = 7.0 Hz, 1H, H2), 3.86 (s, 3H, H8'), 3.81 (s, 3H, H8), 1.77 (d, ³J_{HH} = 7.0 Hz, 3H, H3) ppm.



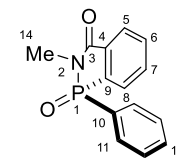
(S)-1-phenyl-2-hydrobenzo[c][1,2]azaphosphol-3-one 1-oxide, (S)-11. By-product obtained from the olefination of **9k**. The *R_P* and *S_P* isomers have been previously characterized.²³ The conditions used for chiral HPLC separation of the enantiomers were:



Daicel Chiralcel OD-H-H column, Hexane/*i*-PrOH = 7/3, flow rate = 0.5 mL/min, *t_R* = 8.8 min (*R_P*), *t_R* = 14.6 min (*S_P*).

2-methyl-1-phenyl-2-hydrobenzo[c][1,2]azaphosphol-3-one 1-oxide, 14. By-product obtained in the olefination of oxaphosphetane **12c**. Yield after precipitation from hexane 99%.

Slightly yellow oil. IR (KBr) ν 1703, 1237 cm⁻¹. ¹H NMR (300.13 MHz, CDCl₃):



δ 8.11 (m, 1H, H5), 7.66-7.82 (m, 5H, H6, H7, H8, H11), 7.64 (m, 1H, H13), 7.52

(m, 2H, H12), 3.02 (d, ³J_{PH} 7.3 Hz, 3H, H14) ppm. ¹³C{¹H} NMR (75.47 MHz, CDCl₃): δ 166.3 (d, ²J_{PC} = 22.2 Hz, C3), 135.2 (d, ²J_{PC} = 8.6 Hz, C4), 133.6 (d, ³J_{PC} = 13.2 Hz, C7), 133.4 (d, ⁴J_{PC} = 2.4 Hz, C6), 133.4 (d, ⁴J_{PC} = 3.1 Hz, C13), 132.2 (d, ²J_{PC} = 11.6 Hz, C11), 131.9 (d, ¹J_{PC} = 118.3 Hz, C9), 129.2 (d, ³J_{PC} = 14.0 Hz, C12), 127.9 (d, ²J_{PC} = 10.2 Hz, C8), 126.6 (d, ¹J_{PC} = 129.8 Hz, C10),

124.9 (d, $^3J_{PC} = 10.3$ Hz, C5), 24.4 (d, $^3J_{PC} = 3.8$ Hz, C14) ppm. $^{31}\text{P}\{^1\text{H}\}$ NMR (121.50 MHz, CDCl_3): δ 26.92 ppm. HRMS (ESI/TOF) m/z : $[\text{M} + 1]$ calcd for $\text{C}_{14}\text{H}_{13}\text{NO}_2\text{P}$, 258.0684; found 258.0675.

General procedure for the determination of rate constants of olefination. The kinetic of the decomposition reaction was monitored by ^{31}P NMR. Samples were prepared by dissolving 10-40 mg of the appropriate spiro-1,2-oxaphosphetane **9/12c** in 0.40-0.45 mL of $\text{DMSO}-d_6$ and heated to 70-160 °C. Inverse-gated NMR spectra (pulse width of 15°, relaxation delay of 7 s) were acquired at specific time intervals (see tables in the Supporting Information). Integration of the spectra afforded the relative concentration of **9**, **11** and **14**.

Acknowledgment. Financial support by the Ministerio de Ciencia e Innovación and FEDER program (projects CTQ2008-117BQU, MAT2006-01997, MAT2010-15094, PTA-2009-2346-I and CSD2006-015, Consolider Ingenio 2010, “Factoría de Cristalización”) are gratefully acknowledged.

Supporting Information Available: Experimental and computational details, characterization data of starting phosphazenes **7c** and **7f** and known compounds **10** and **11**, rate constants measured, determination of ρ for compounds **9c,f,g,h**, Cartesian coordinates and energies of the stationary points located, NBO charges of selected atoms and groups of atoms, and crystallographic data for *cis*-**9d**, *trans*-**9k** and **12a**. This information is available free of charge via the Internet at <http://pubs.acs.org/>.

References

- (1) Staudinger, H.; Meyer, J. Ueber neue organische Phosphorverbindungen III. Phosphinmethylderivate und Phosphinimine. *Helv. Chim. Acta* **1919**, 2, 635–646.
- (2) Wittig, G.; Geissler, G. Zur Reaktionsweise des Pentaphenyl-phosphors und einiger Derivate. *Liebigs Ann. Chem.* **1953**, 580, 44–57.
- (3) (a) Kolodiazhnyi, O. I. *Phosphorus Ylides: Chemistry and Applications in Organic Chemistry*; Wiley-VCH: New York, 1999. (b) Soto, A. P.; García-Álvarez, J. Phosphorus Ylides and Related Compounds. In *Organophosphorus Chemistry: From Molecules to Applications*; Iaroshenko, V., Ed.; Wiley-VCH: Weinheim, 2019; pp 113–162.

1
2
3 (4) For recent reviews, see: (a) Rocha, D. H. A.; Pinto, D. C. G. A.; Silva, A. M. S. Applications
4 of the Wittig Reaction on the Synthesis of Natural and Natural-Analogue Heterocyclic Compounds.
5 *Eur. J. Org. Chem.* **2018**, 2443–2457. (b) Karanam, P.; Reddy, G. M.; Lin, W. Strategic Exploitation
6 of the Wittig Reaction: Facile Synthesis of Heteroaromatics and Multifunctional Olefins. *Synlett*
7 **2018**, 29, 2608–2622. (c) Vik, A.; Hansen, T. V. Synthetic Manipulations of Polyunsaturated Fatty
8 Acids as a Convenient Strategy for the Synthesis of Bioactive Compounds. *Org. Biomol. Chem.*
9 **2018**, 16, 9319–9333. (d) Longwitz, L.; Werner, T. Recent Advances in Catalytic Wittig-type
10 Reactions Based on P(III)/P(V) Redox Cycling. *Pure Appl. Chem.* **2019**, 91, 95–102. (e) Heravi, M.
11 M.; Ghanbarian, M.; Zadsirjan, V.; Alimadadi-Jani, B. Recent Advances in the Applications of
12 Wittig Reaction in the Total Synthesis of Natural Products Containing Lactone, Pyrone, and Lactam
13 as a Scaffold. *Monatsh. Chem.* **2019**, 150, 1365–1407. (f) Eschliman, K.; Bossmann, S. H. Synthesis
14 of Isothiocyanates: An Update. *Synthesis* **2019**, 51, 1746–1752. (g) Zhang, K.; Lu, L.-Q.; Xiao, W.-
15 J. Recent Advances in the Catalytic Asymmetric Alkylation of Stabilized Phosphorous Ylides.
16 *Chem. Commun.* **2019**, 55, 8716–8721.

17
18 (5) Byrne, P. A.; Gilheany, D. G. The Modern Interpretation of the Wittig Reaction Mechanism.
19 *Chem. Soc. Rev.* **2013**, 42, 6670–6696.

20
21 (6) (a) Schlosser, M.; Schaub, B. Cis Selectivity of Salt-Free Wittig Reactions: a "Leeward
22 Approach" of the Aldehyde at the Origin? *J. Am. Chem. Soc.* **1982**, 104, 5821–5823. (b) Vedejs, E.;
23 Marth, C. F. Mechanism of the Wittig Reaction: the Role of Substituents at Phosphorus. *J. Am.*
24 *Chem. Soc.* **1988**, 110, 3948–3958. (c) Vedejs, E.; Fleck, T. J. Kinetic (not Equilibrium) Factors are
25 Dominant in Wittig Reactions of Conjugated Ylides. *J. Am. Chem. Soc.* **1989**, 111, 5861–5871. (d)
26 Robiette, R.; Richardson, J.; Aggarwal, V. K.; Harvey, J. N. On the Origin of High E Selectivity in
27 the Wittig Reaction of Stabilized Ylides: Importance of Dipole–Dipole Interactions. *J. Am. Chem.*
28 *Soc.* **2005**, 127, 13468–13469.

1
2
3 (7) (a) Vedejs, E.; Peterson, M. J. Stereochemistry and Mechanism in the Wittig Reaction. *Top.*
4 *Stereochem.* **1994**, *21*, 1–157. (b) Vedejs, E.; Peterson, M. J. The Wittig Reaction: Stereoselectivity
5 and a History of Mechanistic Ideas (1953–1995). *Adv. Carbanion Chem.* **1996**, *2*, 1–85.
6
7

8
9
10 (8) Stępień, M. Anomalous Stereoselectivity in the Wittig Reaction: The Role of Steric
11 Interactions. *J. Org. Chem.* **2013**, *78*, 9512–9516.
12
13

14
15 (9) Robiette, R.; Richardson, J.; Aggarwal, V. K.; Harvey, J. N. Reactivity and Selectivity in the
16 Wittig Reaction: A Computational Study. *J. Am. Chem. Soc.* **2006**, *128*, 2394–2409.
17
18

19
20 (10) (a) Reitz, A. B.; Mutter, M. S.; Maryanoff, B. E. Observation of Cis and Trans
21 Oxaphosphetanes in the Wittig Reaction by High-Field Phosphorus-31 NMR Spectroscopy. *J. Am.*
22 *Chem. Soc.* **1984**, *106*, 1873–1875. (b) Maryanoff, B. E.; Reitz, A. B.; Mutter, M. S.; Inners, R. R.;
23 Almond, H. R., Jr. Detailed Rate Studies on the Wittig Reaction of Nonstabilized Phosphorus Ylides
24 via Phosphorus-31, Proton, Carbon-13 NMR Spectroscopy. Insight into Kinetic vs. Thermodynamic
25 Control of Stereochemistry. *J. Am. Chem. Soc.* **1985**, *107*, 1068–1070. (c) Maryanoff, B. E.; Reitz,
26 A. B.; Mutter, M. S.; Inners, R. R.; Almond, H. R.; Whittle, R. R.; Olofson, R. A. Stereochemistry
27 and Mechanism of the Wittig Reaction. Diastomeric Reaction Intermediates and Analysis of the
28 Reaction Course. *J. Am. Chem. Soc.* **1986**, *108*, 7664–7678.
29
30
31
32
33
34
35
36
37
38

39
40 (11) For recent examples see: (a) Byrne, P.A.; Muldoon, J.; Ortin, Y.; Müller-Bunz, H.;
41 Gilheany, D. G. Investigations on the Operation of Stereochemical Drift in the Wittig Reaction by
42 NMR and Variable-Temperature NMR Spectroscopy of Oxaphosphetane Intermediates and Their
43 Quench Products. *Eur. J. Org. Chem.* **2014**, 86–98. (b) Uchiyama, Y.; Ohtsuki, T.; Murakami, R.;
44 Shibata, M.; Sugimoto, J. (*E*)-Selective Wittig Reactions between a Nonstabilized Phosphonium
45 Ylide Bearing a Phosphastibatriptycene Skeleton and Benzaldehydes. *Eur. J. Org. Chem.* **2017**,
46 159–174. (c) Uchiyama, Y.; Kuniya, S.; Watanabe, R.; Ohtsuki, T. Heteroatom Effects toward
47 Isomerization of Intermediates in Wittig Reactions of Non-Stabilized Phosphonium Ylides Bearing
48 a Phosphaheteratriptycene Skeleton with Benzaldehyde. *Heteroat. Chem.* **2018**, *29*, e21473. (d)
49 Uchiyama, Y.; Kuniya, S.; Watanabe, R.; Ohtsuki, T. Observation of Intermediates in Wittig
50
51
52
53
54
55
56
57
58
59
60

1
2
3 Reactions of Non-Stabilized Phosponium Ylides Bearing a Phosphaheteratriptycene Skeleton
4
5 Containing Group 15 Elements with Benzaldehyde. *Phosphorus, Sulfur Silicon Relat. Elem.* **2019**,
6
7 *194*, 281-284.

8
9
10 (12) Vedejs, E.; Snoble, K. A. J. Direct Observation of Oxaphosphetanes from Typical Wittig
11
12 Reactions. *J. Am. Chem. Soc.* **1973**, *95*, 5778–5780.

13
14 (13) (a) Vedejs, E.; Meier, G. P.; Snoble, K. A. J. Low-Temperature Characterization of the
15
16 Intermediates in the Wittig Reaction. *J. Am. Chem. Soc.* **1981**, *103*, 2823–2831. (b) Vedejs, E.;
17
18 Marth, C. F. Mechanism of Wittig Reaction: Evidence against Betaine Intermediates. *J. Am. Chem.*
19
20 *Soc.* **1990**, *112*, 3905–3909. (c) Vedejs, E.; Marth, C. F.; Ruggeri, R. Substituent Effects and the
21
22 Wittig Mechanism: the Case of Stereospecific Oxaphosphetane Decomposition. *J. Am. Chem. Soc.*
23
24 **1988**, *110*, 3940–3948.

25
26 (14) (a) López-Ortiz, F.; García-López, J.; Álvarez-Manzaneda, R.; Pérez-Álvarez, I. Isolable
27
28 1,2-Oxaphosphetanes. From Curiosities to Starting Materials for the Synthesis of Olefins. *MiniRev.*
29
30 *Org. Chem.* **2004**, *1*, 65–76. (b) Kolodiazhna, A. O.; Kolodiazhnyi, O. I. Synthesis, Properties and
31
32 Stereochemistry of 2-Halo-1,2 λ^5 -oxaphosphetanes. *Molecules* **2016**, *21*, 1371.

33
34 (15) Birum, G. H.; Matthews, C. N. Reactions of Triphenyl-2,2-bis(trifluoromethyl)vinyl-
35
36 idenephosphorane, Synthesized from a Cyclic Ylide-Ketone Adduct. *J. Org. Chem.* **1967**, *32*, 3554–
37
38 3559.

39
40 (16) Ul-Haque, M.; Caughlan, C. N.; Ramirez, F.; Pilot, J. F.; Smith, C. P. Crystal and Molecular
41
42 Structure of a Four-Membered Cyclic Oxyphosphorane with Pentavalent Phosphorus,
43
44 $\text{PO}_2(\text{C}_6\text{H}_5)_2(\text{CF}_3)_4\text{C}_3\text{H}_2$. *J. Am. Chem. Soc.* **1971**, *93*, 5229–5235.

45
46 (17) Appel, M.; Blaurock, S.; Berger, S. A Wittig Reaction with 2-Furyl Substituents at the
47
48 Phosphorus Atom: Improved (Z) Selectivity and Isolation of a Stable Oxaphosphetane Intermediate.
49
50 *Eur. J. Org. Chem.* **2002**, 1143–1148.

1
2
3 (18) Kawashima, T.; Kato, K.; Okazaki, R. A Novel Synthetic Route to Isolable Pentacoordinate
4 1,2-Oxaphosphetanes and Mechanism of their Thermolysis, the Second Step of the Wittig Reaction.
5
6 *J. Am. Chem. Soc.* **1992**, *114*, 4008–4010.
7

8
9
10 (19) García-López, J.; Peralta-Pérez, E.; Forcén-Acebal, A.; García-Granda, S.; López-Ortiz, F.
11 Dilithiated Phosphazenes: Scaffolds for the Synthesis of Olefins through a New Class of Bicyclic
12 1,2-Oxaphosphetanes. *Chem. Commun.* **2003**, 856–857.
13
14

15
16
17 (20) Dellus, N.; Kato, T.; Bagán, X.; Saffron-Merceron, N.; Branchadell, V.; Baceiredo, A. An
18 Isolable Mixed P,S-Bis(ylide) as an Asymmetric Carbon Atom Source. *Angew. Chem., Int. Ed.* **2010**,
19
20
21
22 *49*, 6798–6801.
23

24 (21) (a) Granoth, I.; Martin, J. C. Hydroxyphosphoranes and Phosphoranoxide Anions -
25 Synthesis, Reactivity, and Acidity of Pentacoordinate Phosphorus acids. *J. Am. Chem. Soc.* **1979**,
26
27
28 *101*, 4618–4622. (b) Perozzi, E. F.; Michalak, R. S.; Figuly, G. D.; Stevenson III, W. H.; Dess, D.
29
30
31 B.; Ross, M. R.; Martin, J. C. Directed Dilithiation of Hexafluorocumyl Alcohol - Formation of a
32
33
34 Reagent for the Facile Introduction of a Stabilizing Bidentate Ligand in Compounds of Hypervalent
35
36
37 Sulfur (10-S-4), Phosphorus (10-P-5), Silicon (10-Si-5), and Iodine (10-I-3). *J. Org. Chem.* **1981**,
38
39 *46*, 1049–1053.

40 (22) (a) Kojima, S.; Sugino, M.; Matsukawa, S.; Nakamoto, M.; Akiba, K.-Y. First Isolation and
41
42
43 Characterization of an Anti-Apicophilic Spirophosphorane Bearing an Oxaphosphetane Ring: A
44
45
46 Model for the Possible Reactive Intermediate in the Wittig Reaction. *J. Am. Chem. Soc.* **2002**, *124*,
47
48
49 7674–7675. (b) Uchiyama, Y.; Kano, N.; Kawashima, T. Syntheses, Structures, and Thermolyses of
50
51
52 Pentacoordinate 1,2-Oxastibetanes: Potential Intermediates in the Reactions of Stibonium Ylides
53
54
55 with Carbonyl Compounds. *J. Org. Chem.* **2006**, *71*, 659–670.

56 (23) García-López, J.; Morán-Ramallal, A.; González, J.; Roces, L.; García-Granda, S.; Iglesias,
57
58
59 M. J.; Oña-Burgos, P.; López-Ortiz, F. Mechanisms of Stereomutation and Thermolysis of *Spiro*-
60
61
62 1,2-oxaphosphetanes: New Insights into the Second Step of the Wittig Reaction. *J. Am. Chem. Soc.*
2012, *134*, 19504–19507.

1
2
3 (24) Kawashima, T.; Kato, K.; Okazaki, R. Synthesis, Structure, and Thermolysis of a 3-
4 Methoxycarbonyl-1, 2 λ^5 -oxaphosphetane. *Angew. Chem., Int. Ed. Engl.* **1993**, *32*, 869–870.

5
6
7 (25) García-López, J.; Fernández, I.; Serrano-Ruiz, M.; López-Ortiz, F. C_{α},C_{ortho} -Dimetalated
8 Phosphazene Complexes. *Chem. Commun.* **2007**, 4674–4676.

9
10 (26) For recent computational work see: (a) Jarwal, N.; Thankachan, P. P. Theoretical Study of
11 the Wittig Reaction of Cyclic Ketones with Phosphorus Ylide. *J. Mol. Model.* **2015**, *21*, 87. (b)
12 Ayub, K.; Ludwig, R. Gas Hydrates Model for the Mechanistic Investigation of the Wittig Reaction
13 “on Water”. *RSC Adv.* **2016**, *6*, 23448–23458. (c) Jarwal, N.; Meena, J. S.; Thankachan, P. P. The
14 *E/Z* Selectivity in Gas Phase Wittig Reaction of Non-Stabilized, Semi-Stabilized and Stabilized
15 Me_3P and Ph_3P Phosphorus Ylides with Monocyclic Ketone: A Computational Study. *Comput.*
16 *Theor. Chem.* **2016**, *1093*, 29–39. (d) Firaha, D. S.; Gibalova, A. V.; Holloczki, O. Basic
17 Phosphonium Ionic Liquids as Wittig Reagents. *ACS Omega* **2017**, *2*, 2901–2911. (e) Adda, A.;
18 Hadjadj-Aoul, R.; Lebsir, F.; Krallafa, A. M. Ab initio Static and Metadynamics Investigations of
19 the Wittig Reaction. *Theor. Chem. Acc.* **2018**, *137*, 94. (f) Farfán, P.; Gómez, S.; Restrepo, A. On
20 the Origins of Stereoselectivity in the Wittig Reaction. *Chem. Phys. Lett.* **2019**, *728*, 153–155. (g)
21 Farfán, P.; Gómez, S.; Restrepo, A. Dissection of the Mechanism of the Wittig Reaction. *J. Org.*
22 *Chem.* **2019**, *84*, 14644–14658.

23
24 (27) Recent calculations support this finding. (a) Kyri, A. W.; Gleim, F.; García Alcaraz, A.;
25 Schnakenburg, G.; Espinosa Ferao, A. Streubel, R. “Low-Coordinate” 1,2-Oxaphosphetanes – a
26 new Opportunity in Coordination and Main Group Chemistry. *Chem. Commun.* **2018**, *54*,
27 7123–7126. (b) Espinosa Ferao, A. On the Mechanism of Trimethylphosphine-Mediated Reductive
28 Dimerization of Ketones. *Inorg. Chem.* **2018**, *57*, 8058–8064. (c) Chamorro, E.; Duque-Noreña, M.;
29 Gutiérrez-Sánchez, N.; Rincón, E.; Domingo, L. R. A Close Look to the Oxaphosphetane Formation
30 along the Wittig Reaction: A [2+2] Cycloaddition? *J. Org. Chem.* **2020**, *85*, 6675–6686.

31
32 (28) Vedejs, E.; Marth, C. F. Oxaphosphetane Pseudorotation: Rates and Mechanistic
33 Significance in the Wittig Reaction. *J. Am. Chem. Soc.* **1989**, *111*, 1519–1520.

(29) For assigning the absolute configuration of a pentacoordinated stereogenic center with a *tbp* geometry see Martin, J. C.; Balthazor, T. M. Sulfuranes. 22. Stereochemical Course of an Associative Displacement at Tetracoordinate Sulfur(IV) in a Sulfurane of Known Absolute Configuration. A Proposed System of Nomenclature for Optically Active Pentacoordinate Species. *J. Am. Chem. Soc.* **1977**, *99*, 152–162.

(30) Repeating three times the decomposition of **9a** at temperatures of 120, 130, 140 and 160 °C afforded *k* values with average deviations of 2, 1, 1, and 1%, respectively. Throughout this study it was assumed that the maximum error of the *k* obtained does not exceed 2%.

(31) Further support to the appearance of a partial positive charge on carbon C4 during olefination was obtained by negative $\rho = -0.22$ ($r = 0.998$) obtained from a Hammett plot for the decomposition of **9c,f,g,h** (Table 1, Figure S5). Hansch, C.; Leo, A.; Taft R. W. A Survey of Hammett Substituent Constants and Resonance and Field Parameters. *Chem Rev.* **1991**, *91*, 165–195.

(32) Berry, R. S. Correlation of Rates of Intramolecular Tunneling Processes, with Application to Some Group V Compounds. *J. Chem. Phys.* **1960**, *32*, 933–938.

(33) Couzijn, E. P. A.; Slootweg, J. C.; Ehlers, A. W.; Lammertsma, K. Stereomutation of Pentavalent Compounds: Validating the Berry Pseudorotation, Redressing Ugi's Turnstile Rotation, and Revealing the Two- and Three-Arm Turnstiles. *J. Am. Chem. Soc.* **2010**, *132*, 18127–18140.

(34) Alternatives exist for improving the accuracy of the results by more extensive consideration of dispersive forces in the calculations. (a) Zhao, Y.; Truhlar, D. G. The M06 Suite of Density Functionals for Main Group Thermochemistry, Thermochemical Kinetics, Noncovalent Interactions, Excited States, and Transition Elements: Two New Functionals and Systematic Testing of Four M06-Class Functionals and 12 Other Functionals. *Theor. Chem. Acc.* **2008**, *120*, 215–241. (b) Grimme, S. Density Functional Theory with London Dispersion Corrections. *WIREs Comput. Mol. Sci.* **2011**, *1*, 211–228.

(35) Gaussian 09, Revision B.01, Frisch, M. J.; Trucks, G. W.; Schlegel, H. B.; Scuseria, G. E.; Robb, M. A.; Cheeseman, J. R.; Scalmani, G.; Barone, V.; Mennucci, B.; Petersson, G. A.; Nakatsuji, H.; Caricato, M.; Li, X.; Hratchian, H. P.; Izmaylov, A. F.; Bloino, J.; Zheng, G.; Sonnenberg, J. L.; Hada, M.; Ehara, M.; Toyota, K.; Fukuda, R.; Hasegawa, J.; Ishida, M.; Nakajima, T.; Honda, Y.; Kitao, O.; Nakai, H.; Vreven, T.; Montgomery, J. A., Jr.; Peralta, J. E.; Ogliaro, F.; Bearpark, M.; Heyd, J. J.; Brothers, E.; Kudin, K. N.; Staroverov, V. N.; Kobayashi, R.; Normand, J.; Raghavachari, K.; Rendell, A.; Burant, J. C.; Iyengar, S. S.; Tomasi, J.; Cossi, M.; Rega, N.; Millam, M. J.; Klene, M.; Knox, J. E.; Cross, J. B.; Bakken, V.; Adamo, C.; Jaramillo, J.; Gomperts, R.; Stratmann, R. E.; Yazyev, O.; Austin, A. J.; Cammi, R.; Pomelli, C.; Ochterski, J. W.; Martin, R. L.; Morokuma, K.; Zakrzewski, V. G.; Voth, G. A.; Salvador, P.; Dannenberg, J. J.; Dapprich, S.; Daniels, A. D.; Farkas, Ö.; Foresman, J. B.; Ortiz, J. V.; Cioslowski, J.; Fox, D. J. Gaussian, Inc., Wallingford CT, 2010.

(36) Jastrzebski, J. T. H.; Boersma, J.; Esch, P. M.; van Koten, G. Intramolecular Penta- and Hexacoordinate Tetraorganotin Compounds Containing the 8-(Dimethylamino)-1-naphthyl Ligand. *Organometallics* **1991**, *10*, 930–935.

(37) (a) Mari, F.; Lahti, P. M.; McEwen, W. E. Molecular Modeling of Oxaphosphetane Intermediates of Wittig Olefination Reactions. *Heteroat. Chem.* **1990**, *1*, 255–259. (b) Yamataka, H.; Nagase, S. Theoretical Calculations on the Wittig Reaction Revisited. *J. Am. Chem. Soc.* **1998**, *120*, 7530–7536.

(38) Restrepo-Cossio, A. A.; Gonzalez, C. A.; Mari, F. Comparative ab Initio Treatment (Hartree–Fock, Density Functional Theory, MP2, and Quadratic Configuration Interactions) of the Cycloaddition of Phosphorus Ylides with Formaldehyde in the Gas Phase. *J. Phys. Chem. A* **1998**, *102*, 6993–7000.

(39) (a) Alagona, G.; Ghio, C. Stepwise versus Concerted Mechanisms in the Wittig Reaction in Vacuo and in THF: The Case of 2,4-Dimethyl-3-pyrrol-1-yl-pentanal and Triphenylphosphonium Ylide. *Theor. Chem. Acc* **2009**, *123*, 337–346. (b) Alagona, G.; Ghio, C. Free Energy Landscapes

1
2
3 in THF for the Wittig Reaction of Acetaldehyde and Triphenylphosphonium Ylide. *Int. J. Quantum*
4
5 *Chem.* **2010**, *110*, 2509–2521.

6
7
8 (40) Marenich, A. V.; Cramer, C. J.; Truhlar, D. G. Universal Solvation Model Based on Solute
9
10 Electron Density and on a Continuum Model of the Solvent Defined by the Bulk Dielectric Constant
11
12 and Atomic Surface Tensions. *J. Phys. Chem. B* **2009**, *113*, 6378–6396.

13
14
15 (41) (a) Vollbrecht, S.; Vollbrecht, A.; Jeske, J.; Jones, P. G.; Schmutzler, R.; du Mont, W.-W.
16
17 Unusual Ring-Closure Reactions During the Oxidation of 1,1'-Bi(3-methyl- phosphol-2-ene) with
18
19 Hexafluoroacetone - Formation of a Tricyclic Fluorine-Containing Phosphorane. *Chem. Ber.* **1997**,
20
21 *130*, 819–822. (b) Kobayashi, J.; Kawashima, T. Chemistry of Pentacoordinated Anti-Apicophilic
22
23 Phosphorus Compounds. *C. R. Chimie* **2010**, *13*, 1249–1259.

24
25
26 (42) (a) Barluenga, J.; Ferrero, M.; López, F.; Palacios, F. Reaction of α -Metallated *N*-Acyl- λ^5 -
27
28 phosphazenes with Aryl Cyanides. *J. Chem. Soc., Perkin Trans. 1* **1989**, 615–618. (b) Barluenga,
29
30 J.; López, F.; Palacios, F. Reactions of *N*-Alkoxy carbonyl Alkyldiphenyl- λ^5 -phosphazenes with
31
32 Acetylene Esters. Synthesis of 1-Aza-2-oxo-4 λ^5 -phosphinines. *J. Organomet. Chem.*
33
34 **1990**, *382*, 61–67.

35
36
37 (43) Álvarez-Gutiérrez, J. M.; Peralta-Pérez, E.; Pérez-Álvarez, I.; López-Ortiz, F. Reactions of
38
39 Lithiated P-Diphenyl(alkyl)(*N*-methoxycarbonyl)phosphazenes with Michael Acceptors and
40
41 Aldehydes. Synthesis of 1*H*-1,2-Azaphosphinin-6-ones, β -Hydroxy(*N*-methoxycarbonyl)phos-
42
43 phazenes and 5,6-Dihydro-1,3,4-oxazaphosphinin-2-ones. *Tetrahedron* **2001**, *57*, 3075–3086.

44
45
46 (44) Bernard, M.; St. Jacques, M. Etude par Résonance Magnétique Nucléaire à Température
47
48 Variable de Composés Apparentés au Méthylèncyclohexane. *Can. J. Chem.* **1970**, *48*, 3039–3044.

49
50
51 (45) Van der Linde, R.; Korver, O.; Korver, P. K.; van der Haak, P. J.; Veenland, J. U.; de Boer,
52
53 Th. J. Proton Magnetic Resonance Spectra of Some 1,1-Diarylalkenes. *Spectrochim. Acta* **1965**, *21*,
54
55 1893–1898.

(46) Sato, M.; Miyaura, N.; Suzuki, A. Stereo- and Regiospecific Synthesis of Trisubstituted Alkenes via the Palladium-catalyzed Cross-coupling Reaction of Diisopropyl (*E*)-(1-Alkyl-1-alkenyl)boronates with Organic Halides. *Chem. Lett.* **1986**, 1329–1332.

(47) Glattfeld, J. W. E.; Milligan, C. H. The Preparation of Optically Active Hydrazines. I. The Preparation of DL-*p*-Trimethylethyl-phenylhydrazine. The Isolation of Pure D-*p*-Trimethylethyl-aniline. *J. Am. Chem. Soc.* **1920**, *42*, 2322–2328.

(48) Boudier, A.; Darcel, C.; Flachsmann, F.; Micouin, L.; Oestreich, M.; Knochel, P. Stereoselective Preparation and Reactions of Configurationally Defined Dialkylzinc Compounds. *Chem. Eur. J.* **2000**, *6*, 2748–2761.

(49) Rapport, I.; Gal, A. Vinylic Cations from Solvolysis. Part XIII. S_N1 and Electrophilic Addition–Elimination Routes in the Solvolysis of α -Bromo- and α -Chloro-4-methoxystyrenes. *J. Chem. Soc., Perkin Trans. 2* **1973**, 301–310.

(50) Bosch, H. W.; Hund, H.-U.; Nietlispach, D.; Salzer, A. General Route to the Half-Open Ruthenium Metallocenes C₅Me₅Ru(pentadienyl) and C₅Me₅Ru(diene)Cl. X-ray Structures of an Optically Active Half-Open Metallocene and of a Dimetallic Ruthenabenzene Complex. *Organometallics* **1992**, *11*, 2087–2098.

(51) Danheiser, R. L.; Nowick, J. S. A Practical and Efficient Method for the Synthesis of β -Lactones. *J. Org. Chem.* **1991**, *56*, 1176–1185.

(52) Wolf, J.; Brandt, L.; Fries, A.; Werner, H. Rhodium-Catalyzed Synthesis of Trisubstituted Olefins from Ethene Derivatives and Diazoalkanes. *Angew. Chem., Int. Ed. Engl.* **1990**, *29*, 510–512.

(53) Hooft, R. W. W. COLLECT, Nonius BV, Delft, The Netherlands, 1998.

(54) Otwinowski, Z.; Minor, W. Processing of X-ray Diffraction Data Collected in Oscillation Mode. *Methods Enzymol.* **1997**, *276*, 307–326.

(55) *Area-Detector Software Package*, SMART & SAINT, Bruker, 2007.

(56) Oxford Diffraction, CrysAlis CCD and CrysAlis RED, Oxford Diffraction Ltd, Abingdon, England, 2006.

(57) Altamore, A.; Cascarano, G.; Giacovazzo, C.; Guagliardi, A.; Burla, M. C.; Polidori, G.; Camalli, M. SIR92 - a Program for Automatic Solution of Crystal Structures by Direct Methods. *J. Appl. Crystallogr.* **1994**, *27*, 435.

(58) Burla, M. C.; Caliendo, R.; Camalli, M.; Carrozzini, B.; Cascarano, G. L.; De Caro, L.; Giacovazzo, C.; Polidori G.; Spagna, R. SIR2004: an Improved Tool for Crystal Structure Determination and Refinement. *J. Appl. Crystallogr.* **2005**, *38*, 381–388.

(59) Beurskens, P. T.; Beurskens, G.; de Gelder, R.; García-Granda, S.; Gould, R. O.; Smits, J. M. M. *The DIRDIF-99 program system*, Technical Report of the Crystallography Laboratory, University of Nijmegen, The Netherlands, 2008.

(60) Parkin, S.; Moezzi, B.; Hope, H. XABS2: an Empirical Absorption Correction Program. *J. Appl. Crystallogr.* **1995**, *28*, 53–56.

(61) Sheldrick, G. M. A Short History of SHELX. *Acta Crystallogr. A* **2008**, *64*, 112–122.

(62) Farrugia, L. J. WinGX Suite for Small-Molecule Single-Crystal Crystallography. *J. Appl. Crystallogr.* **1999**, *32*, 837–838.

(63) Allen, F. H.; Johnson, O.; Shields, G. P.; Smith, B. R.; Towler, M. CIF Applications. XV. enCIFer: a Program for Viewing, Editing and Visualizing CIFs. *J. Appl. Crystallogr.* **2004**, *37*, 335–338.

(64) (a) Spek, A. L. PLATON, An Integrated Tool for the Analysis of the Results of a Single Crystal Structure Determination. *Acta Crystallogr. A* **1990**, *46*, C34. (b) Spek, A. L. PLATON, A *Multipurpose Crystallographic Tool*, Utrecht University, Utrecht, The Netherlands, 1998.

(65) Farrugia, L. J. ORTEP-3 for Windows - a Version of ORTEP-III with a Graphical User Interface (GUI). *J. Appl. Crystallogr.* **1997**, *30*, 565.

(66) Glendening, E. D.; Reed A. E.; Carpenter, J. E.; Weinhold, F. NBO Version 3.1.

1
2
3 (67) (a) Rassolov, V. A.; Ratner, M. A.; Pople, J. A.; Redfern, P. C.; Curtiss, L. A. 6-31G* Basis
4 Set for Third-Row Atoms. *J. Comput. Chem.* **2001**, *22*, 976–984. (b) Zhao, Y.; Truhlar, D. G. A
5
6 New Local Density Functional for Main-Group Thermochemistry, Transition Metal Bonding,
7
8 Thermochemical Kinetics, and Noncovalent Interactions. *J. Chem. Phys.* **2006**, *125*, 194101.
9
10

11
12 (68) (a) González, C.; Schlegel, H. B. An Improved Algorithm for Reaction Path Following. *J.*
13
14 *Chem. Phys.* **1989**, *90*, 2154–2161. (b) González, C.; Schlegel, H. B. Reaction Path Following in
15
16 Mass-Weighted Internal Coordinates. *J. Chem. Phys.* **1990**, *94*, 5523–5527.
17
18

19 (69) *Trans/cis* descriptors indicate the relative orientation of the methyl group and *P*-phenyl
20
21 groups.
22
23
24
25
26
27
28
29
30
31
32
33
34
35
36
37
38
39
40
41
42
43
44
45
46
47
48
49
50
51
52
53
54
55
56
57
58
59
60